



**CROSSTALK-AWARE DESIGN OF ANTI-ALIAS  
FILTERS FOR 3-D AUTOMULTISCOPIC  
DISPLAYS**

*ASHISH JAIN*

Thesis submitted in partial fulfillment  
of the requirements for the degree of  
Master of Science

**BOSTON  
UNIVERSITY**



BOSTON UNIVERSITY  
COLLEGE OF ENGINEERING

Thesis

**CROSSTALK-AWARE DESIGN OF ANTI-ALIAS FILTERS  
FOR 3-D AUTOMULTISCOPE DISPLAYS**

by

**ASHISH JAIN**

B.Tech., Indian Institute of Technology, Kharagpur

Submitted in partial fulfillment of the  
requirements for the degree of  
Master of Science

2006



Approved by

First Reader

---

Janusz Konrad, Ph.D.  
Associate Professor of Electrical and Computer Engineering

Second Reader

---

Prakash Ishwar, Ph.D.  
Assistant Professor of Electrical and Computer Engineering

Third Reader

---

Maja Bystrom, Ph.D.  
Associate Professor of Electrical and Computer Engineering



## Acknowledgments

I would like to sincerely thank my advisor, Professor Janusz Konrad, for his constant support, encouragement, and guidance throughout my graduate program. I am also very thankful to him for all his constructive suggestions and immense care. In spite of his busy schedule he was always accessible to me for discussion and it is not possible for me to put his contribution in few words.

I wish to thank to all members of the Visual Information Processing Laboratory, especially Serdar, for their support and cooperation. I would also like to thank StereoGraphics Corporation for providing Synthagram monitor and its specification used in this research. I would also like to thank Professor Prakash Ishwar for his discussions on crosstalk cancellation algorithm and my committee members, Professor Maja Bystrom and Prof. Ishwar, for reading my thesis.

I would also like to thank my friends and roommates for making my life smooth and enjoyable in Boston, and special thanks to my friend Rahul Ranjan for his constant moral support and patiently listening to my problems.

I am also grateful to all my family members, my father and mother for being constant source of inspiration and my brother for supporting me all my life.



# CROSSTALK-AWARE DESIGN OF ANTI-ALIAS FILTERS FOR 3-D AUTOMULTISCOPIC DISPLAYS

ASHISH JAIN

## ABSTRACT

Automultiscopic displays present a three-dimensional image to viewer without using any eyewear unlike some other three-dimensional display technologies. The absence of glasses and multi-user delivery of content are making the automultiscopic displays popular in the areas of 3D medical imaging, computer games, 3D web browsing, and 3D home entertainment.

The data rendering process required to display a 3D image on automultiscopic screen requires downsampling a 2D regularly-sampled image to 2D irregularly-sampled image. This may result in aliasing and create visual artifacts, which may be unpleasant to the eyes. To avoid this, the image needs to be filtered before downsampling. The bandwidth of the filter needed can be computed in multiple ways one of which is by modeling an irregular sampling structure using an orthogonal lattice. Another method is modeling such a structure using non-orthogonal lattice or union of cosets. The results cited in the literature suggest, however, that the filter bandwidth actually needed is more than the bandwidth computed using the above methods.

The above methods of computing filter bandwidth ignore the fact that there is always some amount of crosstalk, due to optics involved, between the adjacent views. Thus, modeling of the view rendering process by simple subsampling on a lattice or union of cosets is inaccurate. In this thesis, we focus on developing new models to incorporate crosstalk between views into the sampling structure. We also propose to exploit the fact that adjacent views, where crosstalk is strong, are highly correlated. This is expected to result in more accurate anti-alias filter designs and a better 3D visual experience.

Image crosstalk between individual views in automultiscopic displays results in double edges at high contrast object boundaries, also known as ghosting. This reduces the visual comfort for the viewer and creates difficulty in fusing the two images. We discuss our efforts to reduce the formation of ghost images in automultiscopic displays.

# Contents

<b>1</b>	<b>Introduction</b>	<b>1</b>
1.1	Human Depth Perception . . . . .	3
1.2	3-D Display Systems . . . . .	4
1.3	Previous Work . . . . .	9
<b>2</b>	<b>Computing Reciprocal Sampling Structures</b>	<b>13</b>
2.1	Reciprocal Sampling Structure . . . . .	13
2.2	Reciprocal Structure . . . . .	14
2.3	Reciprocal Structure of Lattice . . . . .	15
2.4	Reciprocal Structure of Union of Cosets . . . . .	19
2.5	Reciprocal Structure of Irregular Sampling Structure . . . . .	22
2.6	Using the Fourier transform for Computing Reciprocal Lattice Structure	23
<b>3</b>	<b>Crosstalk-Aware Sampling Structure</b>	<b>29</b>
3.1	Sampling Model for Automultiscopic Displays . . . . .	29
3.2	Perceived Sampling . . . . .	32
3.3	Computing Filter Bandwidth Using Image Covariance Models . . . . .	36
<b>4</b>	<b>Design of Anti-alias Filters</b>	<b>41</b>
4.1	Measurement of Crosstalk . . . . .	41
4.2	Perceived Sampling Structure . . . . .	45
4.3	Computing Reciprocal Structure . . . . .	47
4.4	Filter Design Results . . . . .	51

<b>5 Crosstalk Cancellation</b>	<b>55</b>
5.1 Crosstalk Model . . . . .	55
5.2 Crosstalk Cancellation Algorithm . . . . .	57
5.3 Applying Crosstalk Cancellation Algorithm . . . . .	62
5.4 Results . . . . .	63
<b>6 Conclusion</b>	<b>65</b>
6.1 Discussion of Results . . . . .	65
6.2 Suggestions for Further Work . . . . .	66
<b>References</b>	<b>69</b>
<b>Curriculum Vitae</b>	<b>73</b>

# List of Tables

4.1	Crosstalk measurements with view 1 as center . . . . .	44
4.2	Crosstalk measurements with view 3 as center. . . . .	45
5.1	Spatially-variant crosstalk measurements with view 1 as center . . . . .	61
5.2	Spatially-variant crosstalk measurements with view 3 as center. . . . .	61



# List of Figures

1·1	Autostereoscopic parallax-barrier display principle (Holliman, 2005). . . .	6
1·2	Autostereoscopic lenticular display principle . . . . .	7
2·1	(a) Orthogonal lattice $\Lambda$ ( $\times$ ) along with the underlying orthonormal lattice $\Gamma$ ( $\cdot$ ), (b) reciprocal structure $\Lambda^*$ ( $\times$ ) to the orthogonal lattice. . . .	25
2·2	(a) Non-orthogonal lattice $\Lambda$ ( $\times$ ) along with underlying orthonormal lattice $\Gamma$ ( $\cdot$ ), (b) reciprocal structure $\Lambda^*$ ( $\times$ ) to the non-orthogonal lattice. .	25
2·3	(a) Union of cosets $\Psi$ ( $\times$ ) along with the underlying orthonormal lattice $\Gamma$ ( $\cdot$ ), (b) reciprocal structure $\Psi^*$ ( $\times$ ) to the union of cosets sampling structure. . . . .	26
2·4	(a) Random sampling structure $\Psi$ ( $\times$ ) along with underlying orthogonal lattice $\Gamma$ ( $\cdot$ ), (b) Reciprocal structure $\Psi^*$ ( $\times$ ) to the random sampling structure. . . . .	27
3·1	Image with crosstalk from other views. Number of views = 4. crosstalk coefficient = 0.5 . . . . .	30
3·2	Image with no crosstalk from other views. Number of views = 4. . . . .	31
3·3	(a) Sampling pattern without crosstalk (b) Sampling pattern with crosstalk	33
3·4	Original and nearest alias signal energy: (a) without crosstalk (b) with crosstalk ( $N = 3$ ) . . . . .	36
3·5	Original and nearest alias signal energy: (a) without crosstalk, filter bandwidth = 0.33 (b) with crosstalk, filter bandwidth = 0.56 . . . . .	39

4-1	Measurement of camera linearity characteristics . . . . .	43
4-2	(a) Sampling structure of red color component of view 1, (b) Percieved sampling structure of red color component of view 1 (For the sake of visual clarity, only neighboring-view samples with crosstalk ratio of 0.1 or more are shown). . . . .	46
4-3	(a) Reciprocal sampling structure, (b) Reciprocal crosstalk-aware sampling structure (For the sake of visual clarity, only locations of spectral replications with the gain of 0.2 or more are used to compute the Voronoi diagram and shown). . . . .	47
4-4	Contour plot of desired (shaded) and designed (contours) magnitude response for a multiplexing model based on irregular sampling in case of lenticular display: (a) with no crosstalk, and (b) with crosstalk. Note the wider passband in the case accounting for display crosstalk. . . . .	53
4-5	Contour plot of (a) desired (shaded) and designed (contours) magnitude response for a multiplexing model based on non-orthogonal lattice; and (b) desired response for model based on union of cosets (zoomed in be a factor of 2). . . . .	54

## Chapter 1

# Introduction

The basic principles of stereoscopic imaging were first introduced by Sir Charles Wheatstone in 1838 (Holliman, 2005). Several stereoscopic devices have been developed since 1838. However there have been no reasonable eyewear-free personal 3-D displays until the early 1990's (Berkel et al., 1996b). Today's personal 3-D displays provide no-glasses multi-view look-around 3-D experience with significantly enhanced image quality as compared to previous-generation technologies. The rapid advances in personal 3-D displays have been possible due to availability of low cost, high resolution LCDs (Liquid Crystal Displays), and low cost desktop image processing hardware.

The basic principle of 3-D displays is to provide stereoscopic images to a viewer allowing each eye to see its own view of a 3-D scene. To deliver a stereoscopic image, all 3-D displays use a technique called *angular* multiplexing. Angular multiplexing is a technique in which a pixel appears to have different characteristics such as color and intensity depending on the relative position of a viewer (Cossairt, 2003). All popular 3-D display technologies such as lenticular displays, parallax barrier, and polarized or shuttered glasses, employ angular multiplexing to deliver stereoscopic images.

Parallax barrier and lenticular technologies provide eyewear-free and multiscope 3-D experience to an observer. Multiscope displays provide multiple views to an observer as compared to two views by stereoscopic displays. Both technologies use a spatial multiplexing technique, as compared to the time multiplexing technique used by shuttered glasses, to provide two different perspectives to each eye. Lenticular technology, like

other technologies based on spatial multiplexing, involves tradeoff between the number of views and resolution of an individual view. For example if the number of views in a lenticular display is increased by a factor of  $N$ , then an individual-view resolution goes down by a factor of  $N$ .

In a lenticular 3-D display having  $N$  individual views, the  $N$  view images are multiplexed to create an image suitable for 3-D presentation (Stereographics, 2003). Since the multiplexed image and individual view images are of the same resolution, we need to subsample individual-view images by a factor of  $N$ . The subsampling of individual-view images would require pre-filtering of individual-view images in order to avoid aliasing in the resulting multi-view image (Konrad and Agniel, 2006). Since the individual-view sampling structure is not periodic, the traditional methods of designing anti-alias filters would result in sub-optimal anti-alias filters. The more suitable approach would be to develop a model which can handle non-periodic sampling structures. Thus, in this thesis, we develop a model which can be used to design optimal anti-alias filters for a non-periodic sampling structure.

In a perfect stereoscopic system, each eye sees only its assigned image. The lenticular technology, like many other stereoscopic technologies, suffers from crosstalk between views. Crosstalk is a phenomenon in which each eye, apart from an intended perspective, sees an image of unwanted perspective views. The crosstalk between two views is due to the inherent optical design of a lenticular display and changes the visual experience of a viewer such as, smoother transition between views, reducing the number of views required, and perceived higher resolution of individual views (Berkel and Clarke, 1997). In this research, we quantify the amount of crosstalk between the views and use it to design an optimal anti-alias filter for a lenticular automultiscopic display, SynthaGram SG202 from Stereographics Corporation.

The optical crosstalk between views present in lenticular displays results in inter-

ocular crosstalk for a viewer. The inter-ocular crosstalk between the views reduces the fusibility of views and influences subjective image quality and visual comfort (Berkel and Clarke, 1997; Yeh and Silverstein, 1990). Berkel and Clarke (Berkel and Clarke, 1997) have proposed a new design for a slanted lenticular automultiscopic display, in which the optical crosstalk between adjacent views does not result in inter-ocular crosstalk, thus increasing the image quality and visual comfort for the viewers. Also there have been efforts by Pommeray (Pommeray et al., 2003), Konrad (Konrad et al., 2000), and Klimenko (Klimenko et al., 2003b; Klimenko et al., 2003a) to reduce the crosstalk between views by preprocessing the individual-view images for different stereoscopic display technologies. In this thesis, we discuss our efforts to reduce inter-ocular crosstalk by preprocessing individual view images.

In the rest of the chapter, we introduce the concepts, principles and terminology used in the area of multi-dimensional sampling, automultiscopic displays, and 3-D display technologies to facilitate easier understanding of this thesis.

## 1.1 Human Depth Perception

Binocular vision along with independent information about the distance and direction of the fixation point allows humans to perceive depth in real world (Berkel and Clarke, 1997; Mayhew and Longuet-Higgins, 1982). The human brain combines the two different perspectives of a scene, provided by two eyes, and creates a mental model of the 3-D world. Apart from binocular depth perception, the human visual system also uses the various monocular depth perception cues described below:

- **Interposition or Occlusion:** Two objects occluding each other allow us to perceive relative depth space between the two objects.
- **Size:** The relative size of the object, with previous knowledge of absolute sizes,

can be used to infer the distance between the objects.

- Motion parallax (Kineopsis): provides a depth cue to user when either he moves his head or the object in the scene moves. The information provided by motion parallax is quite similar to the one provided by binocular vision but is not the same. (Berkel and Clarke, 1997; Rogers and Graham, 1982).
- Accommodation: Oculomotor depth cues are due to change in focal length of an eye by using muscles involved in controlling the eye's lens. Oculomotor is a nerve controlling eye movements.

Apart from the depth cues mentioned so far, other cues such as light and shade, texture gradient, and aerial perspective also help a user to judge depth in a scene. Some of these monocular cues can be used by 2-D displays to provide feeling of depth in 2-D images but others like motion parallax are difficult to integrate into 2-D displays.

The most important depth cue for a human visual system is the stereopsis or binocular disparity. Each eye is presented with a different perspective of the same scene based on its location. The two images are fused together to form a 3-D image in the human brain and to provide the feeling of depth to a viewer.

Wheatstone, in 1838, first established that it is possible to create depth sensation by showing each eye a separate 2-D image (Holliman, 2005). The two images should be of the same scene from slightly different viewpoints. He demonstrated this effect by building the first stereoscopic device. Since then many stereoscopic devices have been developed achieving different level of success.

## 1.2 3-D Display Systems

Many 3-D displays have been developed to date; some have reached the consumer market while others have remained in research laboratories. We now review 3-D displays, both

eyewear-equipped and eyewear-free technologies, which had reasonable success in the 3-D stereoscopic devices arena.

- One of the oldest, patented by Louis Ducosdu Hauron in 1891, and most popular technique to deliver 3-D content is anaglyph imaging. Two perspectives of a scene are projected or printed together as a single image, one perspective through red color (usually right view) and the other perspective through a contrasting color such as blue, green or cyan (usually left view). When an anaglyph image is viewed through appropriate colored glasses, each eye sees its own perspective thereby creating a 3-D effect (Dubois, 2001). The anaglyph method is the only method which can be used to display stereoscopic images on normal 2-D displays and also in print. This technique has been quite popular in 3-D comic strips and movies.
- Another popular technique used in 3-D content delivery is using polarized glasses to separate multiplexed views. In this method, two different images are projected onto the same screen through orthogonal polarizing filters. The viewer uses low-cost glasses of appropriate polarization to separate the two views. This technique has been the most popular in delivering 3-D movies. Recently “Polar express” was released using polarized 3-D glasses, reviving interest in 3-D movies.
- Another popular technique is using time-sequential shuttered glasses in which active LCS (Liquid Crystal Shutter) is used for view separation. The images are presented at the rate of 120 frames per second by time-multiplexing left and right views each captured at 60 Hz. The left and right shutters are synchronized with a monitor so that each eye gets its own view. These displays suffer from crosstalk between individual views due to phosphor persistence, LCS leakage, and LCS shutter timing errors. Konrad et al (2000) proposed pre-processing individual-view images so as to reduce the inter-ocular crosstalk.

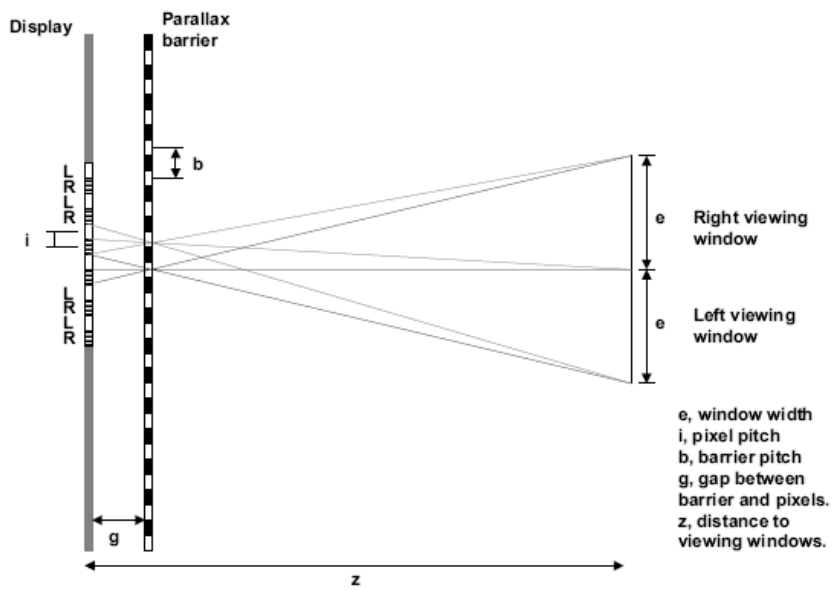


**Figure 1.1:** Autostereoscopic parallax-barrier display principle (Holli-man, 2005).

- Parallax-barrier displays: In this display technology, a parallax barrier is placed on a display in such a way that half of the pixels are seen by left eye and the other half by right eye. The left and right images are interlaced in columns as shown in Fig. 1-1. The display can be used for more than one viewer, albeit with reduced image quality, because the viewing window is repeated periodically in the space in front of the display. These displays suffer from reduced brightness, reflection off of the glass surface of parallax barrier, and diffraction. The use of bright light sources and anti-reflection coated optics has solved the first two problems (Holliman, 2005).

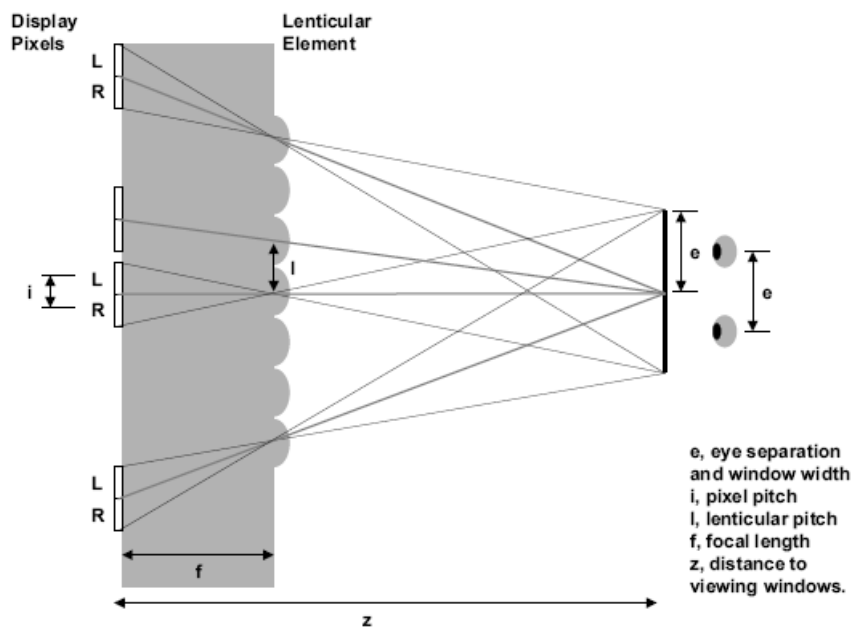


**Figure 1-2:** Autostereoscopic lenticular display principle (Holliman, 2005)

- Lenticular displays: These displays have cylindrical lenses placed over the screen of 2-D displays such as an LCD. The lenses, placed over LCD, diffuse light from each pixel in such a way that each eye sees its perspective of a scene (Berkel et al., 1996a). Fig. 1-2 shows a two-view autostereoscopic lenticular display. A lenticular automultiscopic display works on the same principle except that the number of views is greater than two. In a multiscopic display, the position of an observer determines the pair of views seen. Several improvements have been made since the first lenticular display was designed. The improved lenticular automultiscopic displays use slanted lenticular sheets, and offer increased number of views, as well as higher resolution of individual views. The lenticular displays still have the disadvantage of repeating view zones, reduced individual view resolution, and crosstalk between views. This latter problem has been solved by designing a display in which optical crosstalk between adjacent views does not manifest itself in inter-ocular crosstalk (Berkel and Clarke, 1997). This can be achieved if a display is designed so that non-adjacent views, for example views 1 and 3, are presented to the left and right eyes respectively. Such a design may suffer from optical crosstalk between the views but reduces inter-ocular crosstalk considerably (Berkel and Clarke, 1997).

The biggest advantage of lenticular displays is that they provide multiple views and hence an observer can experience "look-around". The number of views in displays available on the market today varies from 4 to 16 (Dodgson, 2005). The number of views greater than two also provides motion-parallax depth cue which is an important monocular depth cue. The greatest advantage of lenticular displays is that they provide multiple views using normal LCD screen and a lenticular sheet. The ever-increasing performance of lenticular displays, due to availability of higher resolution LCDs and cheaper high-performance graphics hardware on desktops make them a viable solution

for the mass market.

### 1.3 Previous Work

In an automultiscopic display, a lenticular sheet made up of microlenses is placed over the display to refract light from pixels into different angular zones in front of the screen. It is possible to map visibility of each pixel on the screen to a particular angular zone. This allows us to spatially multiplex view images in a way that each eye sees a particular view image. However, due to the downsampling process associated with spatial multiplexing of images, aliasing effects such as *Moiré* patterns, spurious color dots, and distorted texture patterns are visible (Konrad and Agniel, 2006). To eliminate the aliasing artifacts, it is necessary that each view image be suitably pre-filtered before multiplexing (Konrad and Agniel, 2003). In early lenticular displays, a lenticular sheet was placed vertically over a pixel-addressable screen. The displays however suffered from two major problems: the resolution of individual views was poor in the horizontal direction and a black mask between pixels was visible between view transitions (Berkel, 1999). Slanting the lenticular sheet at a small angle can solve both problems. The slanting of lenticular sheet makes the black mask equally visible from every position thereby making it invisible to the observer. Similarly, slanting allows a designer to achieve a balance between horizontal and vertical resolutions of each view. Another advantage of slanting the lenticular sheet is that the view flipping becomes a continuous process so that there are no visible boundaries between the views that would otherwise exist (Berkel and Clarke, 1997).

The advantages offered by using a slanted lenticular sheet make it a desirable design feature in lenticular automultiscopic display designs. However, making a lenticular sheet slanted makes the individual view pixel distribution irregular. This irregularity in pixel distribution for each view makes the downsampling process, inherent in the multiplexing

of images, quite complicated. The multiplexing of images now requires an image to be downsampled from an orthogonal sampling grid to an irregular sampling grid.

The anti-alias filter design for downsampling an image from an orthogonal sampling grid to another orthogonal sampling grid is trivial and has been discussed widely in literature. Dubois (Dubois, 1985) first introduced the method to design an anti-alias filter for a downsampling process in which an image is being downsampled from a regular sampling grid to another regular sampling grid. He introduced the concept of sampling structures based on lattices and used the concept to develop a framework in which sampling structure conversion along with anti-aliasing filter design was possible. The sampling structures which Dubois dealt with were limited to regular sampling structures.

However, the view pixels in slanted lenticular displays are far from regular. With this problem in mind, Konrad and Agniel developed a design method in which an irregular sampling structure was approximated with regular sampling structures such as orthogonal lattices (Konrad and Agniel, 2003), non-orthogonal lattices (Konrad and Agniel, 2004) and a union of cosets (Konrad and Agniel, 2006).

In this research, they developed a cost function to measure how close a regular sampling structure model was to an irregular sampling structure. An exhaustive search was performed to minimize the cost function by varying the model parameters. Once an approximate regular sampling structure was found, a design of an anti-alias filter was performed using the multidimensional signal processing theory developed by Dubois (Dubois, 1985). The anti-alias filters designed were found to be quite effective in removing aliasing artifacts from multiplexed images. Since the method proposed by Konrad and Agniel performs an exhaustive search of parameters, the computational complexity of designing a filter is quite high (Agniel, 2004). Also the method involves approximating an irregular sampling structure with a regular sampling structure. It is desirable to have a filter design process where the amount of computational complexity associated

with the design is reduced and irregular sampling structures are handled directly.

In an ideal stereoscopic device, the right eye should only see a right-eye image and no left-eye image, and vice versa for the left eye. For a real stereoscopic system, this is not true. Some amount of the left-eye image is seen by the right eye and vice versa. The amount and source of crosstalk varies from system to system (Pommeray et al., 2003). For example, time-sequential displays suffer from crosstalk due to phosphor persistence and shutter leakage, whereas lenticular displays suffer from crosstalk due to optics. The crosstalk between views reduces image quality, causes eye strain and headache to an observer and influences conspicuity of ghost images at object boundaries. The conspicuity of ghost images is also more prominent for an image with bright region against a dark background (Pommeray et al., 2003). Hsu (Hsu et al., 1994) proposed that crosstalk is visible only if it is different from stimuli by more than 14 percent. There have been efforts to reduce crosstalk by using short phosphor persistence in liquid crystal (LC) shutter glasses systems (Woods and Tan, 2002). Another approach taken by Berkel (Berkel and Clarke, 1997) to reduce crosstalk in lenticular display systems is to project non-adjacent views on left and right eye. This method does not reduce the optical crosstalk between the views but reduces the inter-ocular crosstalk.

The idea to reduce crosstalk by pre-processing view images was first proposed by Lipscomb in 1994 (Lipscomb and Wooten, 1994). The method suggested was to raise the background from black to grey and subtract the ghosts before the projection of images onto the screen. The technique was fairly successful in eliminating ghosts. Similar crosstalk cancellation techniques were proposed by Kilmenko (Klimenko et al., 2003a) and Pommrey (Pommeray et al., 2003) for polarized glasses. Pommrey, apart from developing a crosstalk cancellation method, also proposed a quantitative measure SGR (signal-to-ghosting ratio) to measure the amount of crosstalk between the views. The research also exploited the fact that the SNR (signal-to-noise ratio) of a stereo pair

with correlated noise is lower than that of a stereo pair with uncorrelated noise. So it is possible to reduce the SNR of individual view images but increase the SGR ratio of stereo images (Pommeray et al., 2003), thereby increasing the overall 3-D quality for an observer. Konrad (Konrad et al., 2000) proposed a method to reduce crosstalk between the views in time-sequential displays. The basic principle is similar to one proposed by Lipscomb (Lipscomb and Wooten, 1994), but the crosstalk measurement is done by psychovisual experiments. Also, the crosstalk model used is non-linear and uses lookup table in its crosstalk cancellation algorithm, making it computationally efficient. The results obtained were quite encouraging in terms of improvement in 3-D visual experience of viewers.

Most of the crosstalk cancellation efforts to date have been restricted to stereoscopic displays. There have been no efforts so far in spatially-multiplexed multiscopic displays. This is because the crosstalk model in spatially-multiplexed multiscopic displays becomes complicated. However, we believe it is worthwhile to study the effectiveness of simple linear crosstalk models in crosstalk cancellation in spatially-multiplexed multiscopic displays.

## Chapter 2

# Computing Reciprocal Sampling Structures

### 2.1 Reciprocal Sampling Structure

The sampling of an image involves specification of image intensity or color over some predefined discrete set of points in 2-D space referred to as sampling structure. One example of periodic sampling structure is a lattice. The predefined periodic sets of points are known as lattices, a term borrowed from solid state physics. The theory of sampling multidimensional signals on a lattice was proposed by Peterson in 1962 and developed further by Gaarder in 1972 (Dubois, 1985). A detailed review of multidimensional sampling theory discussing sampling of multidimensional signals, Fourier transform representations, sampling of continuous signals, and conversion between different sampling structures was done by Dubois (Dubois, 1985). The sampling of images has been satisfactorily studied as the multiplication of the continuous signals by a predefined train of Dirac delta functions. A very important concept in multidimensional sampling theory is the concept of reciprocal lattice (Dubois, 1985). The idea of reciprocal lattice makes the frequency domain representation simpler. The method to compute reciprocal lattice was developed by Dubois for regular lattices such as orthogonal lattices, non-orthogonal lattices, and union of cosets. Later, Konrad and Agniel (Konrad and Agniel, 2006) presented a method to compute reciprocal structure for irregular sampling structure by approximating the irregular sampling structure using union of cosets. The proposed method could compute the reciprocal lattice for irregular sampling structure approxi-

mately but was a computationally demanding procedure. In this chapter, we introduce and develop a generic method to compute reciprocal lattice which works for lattices, unions of cosets and irregular sampling structures. The method is not only computationally less complex for irregular sampling structures than the method proposed by Konrad and Agniel (Konrad and Agniel, 2006) but also computes a mathematically accurate reciprocal structure. We propose the idea of using Fourier transform to compute an accurate reciprocal structure. We first prove that computing the 2D Fourier transform of a sampling structure, in the case of orthogonal lattice, indeed results in reciprocal lattice structure and we also prove that it works for union of cosets. In the following section, we demonstrate that 2D transform of lattice structure results in corresponding reciprocal lattice structure.

## 2.2 Reciprocal Structure

A lattice  $\Gamma$  in  $\mathbf{R}^N$  is the set of all linear combinations of basis vectors  $\mathbf{v}_1, \mathbf{v}_2, \dots, \mathbf{v}_N$  with integer coefficients.

$$\Gamma = \{n_1\mathbf{v}_1 + n_2\mathbf{v}_2 + \dots + n_N\mathbf{v}_N : n_i \in Z, i = 1, 2, \dots, N\} \quad (2.1)$$

The quantity  $d(\Gamma)$ , determinant of the lattice  $\Gamma$ , physically represents the reciprocal of the sampling density. The definition of reciprocal lattice as defined in (Dubois, 1985) is “Given a lattice  $\Gamma$ , the set of all vectors  $\mathbf{y}$  such that  $\mathbf{y}^T \mathbf{x}$  is an integer for all  $\mathbf{x} \in \Gamma$  is called the reciprocal lattice  $\Gamma^*$  of the lattice  $\Gamma$ .” Dubois also proved that a signal sampled on  $\Gamma$  would have its frequency spectrum replicated at each point in  $\Gamma^*$ .

The definition of reciprocal structure was left open for sampling structure other than lattices and unions of cosets. In this section, we introduce the concept of reciprocal structure in general case including, lattices and union of cosets. Let  $u(\mathbf{x})$  be a real-time continuous signal and  $U(\mathbf{f})$  be its frequency spectrum. If we sample a real-time

continuous signal  $u(\mathbf{x})$  on sampling structure  $\Psi$ , then

$$u(\mathbf{x})\phi(\mathbf{x}) = u_s(\mathbf{x}) \quad (2.2)$$

This means  $\phi(\mathbf{x})$  is a signal which is non-zero at the points  $\mathbf{x} \in \Psi$ . The spectrum of sampled signal  $u_s(\mathbf{x})$  must be periodic in nature. Let  $U_s(\mathbf{f})$  be the spectrum of the sampled signal, then we have

$$U(\mathbf{f}) * \Phi(\mathbf{f}) = U_s(\mathbf{f}) \quad (2.3)$$

where  $*$  denotes convolution, and we can define a reciprocal structure  $\Psi^*$  as a set of vectors  $\mathbf{f}$  for which  $\Phi(\mathbf{f})$  is non-zero. Each point  $\mathbf{f}$  in reciprocal structure is associated with gain of  $\Phi(\mathbf{f})$ . Mathematically,

$$\Psi^* = \{\mathbf{f}; \Phi(\mathbf{f}) \neq 0, \mathbf{f} \in R^N\} \quad (2.4)$$

This definition of reciprocal structure is consistent with the definition of reciprocal structure for lattices and unions of cosets (Dubois, 1985) and can be used to define reciprocal structure for an arbitrary sampling structure. The gain values in the case of reciprocal lattice would be 1 and can be ignored. We will use this definition of reciprocal sampling structure in this thesis. Using equation (2.3) and (2.2), we claim that it is possible to compute reciprocal structure by calculating Fourier transform of signal  $\phi(\mathbf{x})$ , which is non-zero at points belonging to the sampling structure  $\Psi$ .

### 2.3 Reciprocal Structure of Lattice

The paper by Dubois (Dubois, 1985) discusses ways to compute the reciprocal structure for lattices and unions of cosets. All the sampling structures discussed by Dubois are periodic in nature (Dubois, 1985). However difficulty arises when the sampling pattern

of an image is not periodic. A method to compute reciprocal structure for an aperiodic sampling structure was proposed by Konrad and Agniel (Konrad and Agniel, 2006). However the method proposed was computationally demanding and gave mathematically approximate solution. In this section, we propose a computationally less expensive, more precise method of computing reciprocal structure of periodic and aperiodic sampling structures. We first develop the method for lattices and then develop it for union of cosets and aperiodic structures.

Let  $\Lambda$  be a lattice of which we want to compute reciprocal lattice. Let  $\Gamma$  be an underlying denser *orthogonal* lattice such that  $\Lambda \subset \Gamma$ ;  $\Gamma, \Lambda \subset R^N$ . Let us define a signal  $\phi(\mathbf{x})$  over lattice  $\Gamma$  as,

$$\phi(\mathbf{x}) = \begin{cases} 1, & \text{for } \mathbf{x} \in \Lambda \\ 0, & \text{for } \mathbf{x} \notin \Lambda, \mathbf{x} \in \Gamma \end{cases} \quad (2.5)$$

The discrete-space Fourier transform of  $\phi(\mathbf{x})$  can be defined as (Dubois, 1985),

$$F\{\phi(\mathbf{x})\}(\mathbf{f}) = \sum_{\mathbf{x} \in \Gamma} \phi(\mathbf{x}) e^{-j2\pi \mathbf{f}^T \mathbf{x}}, \quad \mathbf{f} \in R^N \quad (2.6)$$

$$F\{\phi(\mathbf{x})\}(\mathbf{f}) = \sum_{\mathbf{x} \in \Lambda} \phi(\mathbf{x}) e^{-j2\pi \mathbf{f}^T \mathbf{x}} + \sum_{\mathbf{x} \notin \Lambda, \mathbf{x} \in \Gamma} \phi(\mathbf{x}) e^{-j2\pi \mathbf{f}^T \mathbf{x}}, \quad \mathbf{f} \in R^N \quad (2.7)$$

Since  $\phi(\mathbf{x}) = 0$  for  $\mathbf{x} \notin \Lambda$ ,  $\mathbf{x} \in \Gamma$ ; we have

$$F\{\phi(\mathbf{x})\}(\mathbf{f}) = \sum_{\mathbf{x} \in \Lambda} \phi(\mathbf{x}) e^{-j2\pi \mathbf{f}^T \mathbf{x}}, \quad \mathbf{f} \in R^N \quad (2.8)$$

As  $\phi(\mathbf{x}) = 1$  for all  $\mathbf{x} \in \Lambda$ , we get

$$F\{\phi(\mathbf{x})\}(\mathbf{f}) = \sum_{\mathbf{x} \in \Lambda} e^{-j2\pi \mathbf{f}^T \mathbf{x}} \quad (2.9)$$

Since  $\mathbf{x}$  is the set of all vectors in lattice  $\Lambda$ , we can write  $\mathbf{x}$  as

$$\mathbf{x} = \mathbf{V}\mathbf{n}$$

where  $V$  is the sampling matrix of  $\Lambda$  and  $\mathbf{n} \in Z^N$ . The sampling matrix  $\mathbf{V}$  is of dimensions  $N \times N$ .

Substituting the value of  $\mathbf{x}$  in equation (2.9) we get,

$$F\{\phi(\mathbf{x})\}(\mathbf{f}) = \sum_{\mathbf{x} \in \Lambda} e^{-j2\pi\mathbf{f}^T\mathbf{V}\mathbf{n}} \quad (2.10)$$

$$F\{\phi(\mathbf{x})\}(\mathbf{f}) = \sum_{\mathbf{n}} e^{-j2\pi(\mathbf{V}^T\mathbf{f})^T\mathbf{n}} \quad (2.11)$$

To simplify equation (2.11), we make the following substitution.

$$\mathbf{V}^T\mathbf{f} = \mathbf{m} \quad (2.12)$$

Since  $\mathbf{f} \in R^N$  and  $\mathbf{V}$  is the sampling matrix of  $\Lambda$ , we must have  $\mathbf{m} \in R^N$ .

$$F\{\phi(\mathbf{x})\}(\mathbf{m}) = \sum_{\mathbf{n}} e^{-j2\pi\mathbf{m}^T\mathbf{n}} \quad (2.13)$$

$$\Phi(\mathbf{m}) = \sum_{\mathbf{n}} e^{-j2\pi\mathbf{m}^T\mathbf{n}} \quad (2.14)$$

Since  $\mathbf{m} = [m_1 m_2 \dots m_N]^T$ ,  $\mathbf{n} = [n_1 n_2 \dots n_N]^T$ , we have

$$= \sum_{n_1} \sum_{n_2} \dots \sum_{n_N} e^{-j2\pi(m_1 n_1 + m_2 n_2 + \dots + m_N n_N)} \quad (2.15)$$

$$= \left( \sum_{n_1} e^{-j2\pi m_1 n_1} \right) \left( \sum_{n_2} e^{-j2\pi m_2 n_2} \right) \dots \left( \sum_{n_N} e^{-j2\pi m_N n_N} \right) \quad (2.16)$$

Now we need to prove that  $\sum_{n_1} e^{-j2\pi m_1 n_1}$  is the same as a train of Dirac delta functions i.e.

$$S(m_1) = \sum_{n_1 \in Z} e^{-j2\pi m_1 n_1} = \sum_{k_1} \delta(m_1 - k_1), \quad k_1 \in Z \quad (2.17)$$

The mathematical proof of this is beyond the scope of this thesis and can be found in introductory book on generalized functions by Zemanian (Zemanian, 1987) and handbook on generalized functions by Zayed (Zayed, 1996).

Using equation (2.16) and equation (2.17) we can write,

$$\Phi(\mathbf{m}) = \sum_{k_1} \delta(m_1 - k_1) \sum_{k_2} \delta(m_2 - k_2) \dots \sum_{k_N} \delta(m_N - k_N), \quad k_1, k_2, \dots, k_N \in Z \quad (2.18)$$

$$\Phi(\mathbf{m}) = \sum_{k_1} \sum_{k_2} \dots \sum_{k_N} \delta(m_1 - k_1) \delta(m_2 - k_2) \dots \delta(m_N - k_N), \quad k_1, k_2, \dots, k_N \in Z \quad (2.19)$$

$$\Phi(\mathbf{m}) = \sum_{k_1} \sum_{k_2} \dots \sum_{k_N} \delta(m_1 - k_1, m_2 - k_2, \dots, m_N - k_N), \quad k_1, k_2, \dots, k_N \in Z \quad (2.20)$$

Using equation (2.14) and (2.20), we get

$$\Phi(\mathbf{m}) = \sum_{\mathbf{n}} e^{-j2\pi \mathbf{m}^T \mathbf{n}} = \sum_{\mathbf{k}} \delta(\mathbf{m} - \mathbf{k}), \quad \mathbf{n} \in Z^N, \quad \mathbf{k} \in Z^N \quad (2.21)$$

Substituting for  $\mathbf{m}$  from equation (2.12), we get

$$\Phi(\mathbf{f}) = \sum_{\mathbf{n}} e^{-j2\pi \mathbf{f}^T \mathbf{V} \mathbf{n}} = \sum_{\mathbf{k}} \delta(\mathbf{V}^T \mathbf{f} - \mathbf{k}), \quad \mathbf{k} \in Z^N \quad (2.22)$$

Using scaling property of Dirac delta function, we get

$$\Phi(\mathbf{f}) = \frac{1}{|\det(\mathbf{V})|} \sum_{\mathbf{k}} \delta(\mathbf{f} - (\mathbf{V}^{-1})^T \mathbf{k}), \quad \mathbf{k} \in Z^N \quad (2.23)$$

This shows that  $\Phi(\mathbf{f})$  is zero everywhere except at values of  $\mathbf{f}$  such that  $\mathbf{f} = (\mathbf{V}^{-1})^T \mathbf{k}$  and  $\mathbf{k} \in \mathbb{Z}^N$ . If we sample any continuous signal over lattice  $\Lambda$ , then the Fourier transform of the sampled signal is the superposition of original spectrum replicated at set of points defined by  $\mathbf{f} = (\mathbf{V}^{-1})^T \mathbf{k}$ . This means that this set of points represents reciprocal structure of lattice  $\Lambda$ . This proves that the discrete-space Fourier transform of signal  $\phi(\mathbf{x})$ , as defined in equation (2.5), results in the corresponding reciprocal lattice structure.

## 2.4 Reciprocal Structure of Union of Cosets

A union of cosets is a sampling structure defined as a union of several shifted lattices. Let  $\Lambda$  and  $\Gamma$  be lattices.  $\Lambda$  is a sublattice of  $\Gamma$  if every point of  $\Lambda$  is also a point of  $\Gamma$ . For any  $\mathbf{c}_i \in \Gamma$ ,  $\mathbf{c}_i \notin \Lambda$ , the set  $\mathbf{c}_i + \Lambda = \{\mathbf{c}_i + \mathbf{x} | \mathbf{x} \in \Lambda\}$  is called a coset of  $\Lambda \in \Gamma$ .

Let us consider a structure  $\Psi$  as a union of selected  $P$  cosets of a sublattice  $\Lambda$  in an orthonormal lattice  $\Gamma$ . Mathematically we can write  $\Psi$  as:

$$\Psi = \bigcup_{i=1}^P (\mathbf{c}_i + \Lambda) \quad (2.24)$$

We define a signal

$$\phi(\mathbf{x}) = \begin{cases} 1, & \text{for } \mathbf{x} \in \Psi \\ 0, & \text{for } \mathbf{x} \notin \Psi, \mathbf{x} \in \Gamma \end{cases} \quad (2.25)$$

The next step is to compute the Fourier transform of the signal  $\phi(\mathbf{x})$  over the orthogonal lattice structure  $\Gamma$ ,

$$\Phi(\mathbf{f}) = \sum_{\mathbf{x} \in \Gamma} \phi(\mathbf{x}) e^{-j2\pi \mathbf{f}^T \mathbf{x}}, \quad \mathbf{f} \in \mathbb{R}^N \quad (2.26)$$

$$\Phi(\mathbf{f}) = \sum_{\mathbf{x} \in \Psi} \phi(\mathbf{x}) e^{-j2\pi \mathbf{f}^T \mathbf{x}} + \sum_{\mathbf{x} \notin \Psi, \mathbf{x} \in \Gamma} \phi(\mathbf{x}) e^{-j2\pi \mathbf{f}^T \mathbf{x}}, \quad \mathbf{f} \in R^N \quad (2.27)$$

Since  $\phi(\mathbf{x}) = 0$  for  $\mathbf{x} \notin \Psi$ ,  $\mathbf{x} \in \Gamma$ , we have

$$\Phi(\mathbf{f}) = \sum_{\mathbf{x} \in \Psi} \phi(\mathbf{x}) e^{-j2\pi \mathbf{f}^T \mathbf{x}}, \quad \mathbf{f} \in R^N \quad (2.28)$$

Using equation (2.24) and (2.28), we can write

$$\Phi(\mathbf{f}) = \sum_{i=1}^P \sum_{\mathbf{x} \in \Lambda} \phi(\mathbf{c}_i + \mathbf{x}) e^{-j2\pi \mathbf{f}^T \mathbf{x}}, \quad \mathbf{f} \in R^N \quad (2.29)$$

Using the time-shift property of the Fourier transform, we get

$$\Phi(\mathbf{f}) = \sum_{i=1}^P e^{j2\pi \mathbf{f}^T \mathbf{c}_i} \sum_{\mathbf{x} \in \Lambda} \phi(\mathbf{x}) e^{-j2\pi \mathbf{f}^T \mathbf{x}}, \quad \mathbf{f} \in R^N \quad (2.30)$$

Since  $\phi(\mathbf{x}) = 1$  for all  $\mathbf{x} \in \Psi$ , we get

$$\Phi(\mathbf{f}) = \sum_{i=1}^P e^{j2\pi \mathbf{f}^T \mathbf{c}_i} \sum_{\mathbf{x} \in \Lambda} e^{-j2\pi \mathbf{f}^T \mathbf{x}}, \quad \mathbf{f} \in R^N \quad (2.31)$$

Since  $\mathbf{x} \in \Lambda$ , we can write  $\mathbf{x} = \mathbf{V}\mathbf{n}$ ,  $\mathbf{n} \in Z^N$ ; where  $\mathbf{V}$  is the sampling matrix of lattice  $\Lambda$

$$\Phi(\mathbf{f}) = \sum_{i=1}^P e^{j2\pi \mathbf{f}^T \mathbf{c}_i} \sum_{\mathbf{n}} e^{-j2\pi \mathbf{f}^T \mathbf{V}\mathbf{n}}, \quad \mathbf{f} \in R^N \quad (2.32)$$

Using equation (2.22) and (2.32), we get

$$\Phi(\mathbf{f}) = \sum_{i=1}^P e^{j2\pi \mathbf{f}^T \mathbf{c}_i} \sum_{\mathbf{k} \in Z^N} \delta(\mathbf{V}^T \mathbf{f} - \mathbf{k}), \quad \mathbf{f} \in R^N \quad (2.33)$$

$$\Phi(\mathbf{f}) = \frac{1}{|\det(\mathbf{V})|} \sum_{i=1}^P e^{j2\pi \mathbf{f}^T \mathbf{c}_i} \sum_{\mathbf{k} \in Z^N} \delta(\mathbf{f} - (\mathbf{V}^{-1})^T \mathbf{k}), \quad \mathbf{f} \in R^N \quad (2.34)$$

$$\Phi(\mathbf{f}) = \begin{cases} \frac{1}{|\det(\mathbf{V})|} \sum_{i=1}^P e^{j2\pi\mathbf{f}^T \mathbf{c}_i}, & \mathbf{f} = (\mathbf{V}^{-1})^T \mathbf{k}, \quad \mathbf{k} \in Z^N \\ 0, & \text{elsewhere.} \end{cases} \quad (2.35)$$

The reciprocal structure is defined as a set of points where replication of spectrum, sampled on  $\Psi$ , happens. For replication of spectrum to happen  $\Phi(\mathbf{f})$  should be non-zero. Therefore, reciprocal structure  $\Psi^*$  can be written as:

$$\Psi^* = \{\mathbf{r} : \Phi(\mathbf{r}) \neq 0, \mathbf{r} \in R^N\} \quad (2.36)$$

Since  $\Phi(\mathbf{r}) = 0$  except for  $\mathbf{r} = (\mathbf{V}^{-1})^T \mathbf{k}$ ,  $\mathbf{k} \in Z^N$ , we can write

$$\Psi^* = \{\mathbf{r} : \Phi(\mathbf{r}) \neq 0, \mathbf{r} = (\mathbf{V}^{-1})^T \mathbf{k}, \mathbf{k} \in Z^N\} \quad (2.37)$$

Since  $\mathbf{r} = (\mathbf{V}^{-1})^T \mathbf{k}$  and  $\mathbf{k} \in Z^N$ , then  $\mathbf{r} \in \Lambda^*$  because  $\mathbf{V}$  is the sampling matrix of lattice  $\Lambda$ . We can write the above expression as follows:

$$\Psi^* = \{\mathbf{r} : \Phi(\mathbf{r}) \neq 0, \mathbf{r} \in \Lambda^*\} \quad (2.38)$$

The reciprocal structure obtained by Dubois (Dubois, 1985) for the same sampling pattern  $\Psi$  being union of selected  $P$  cosets of a sublattice  $\Lambda$  in a lattice  $\Gamma$ , is as follows:

$$\Psi^* = \{\mathbf{r} : g(\mathbf{r}) \neq 0, \mathbf{r} \in \Lambda^*\} \quad (2.39)$$

where  $g(\mathbf{r}) = \frac{1}{|\det(\mathbf{V})|} \sum_{i=1}^P e^{j2\pi\mathbf{r}^T \mathbf{c}_i}$ .

We compare the reciprocal structure of  $\Psi$  obtained by computing the Fourier transform of signal  $\phi(\mathbf{x})$  in equation (2.38) with the one obtained by Dubois in equation (2.39). We see that both are defined over a set of vectors  $\mathbf{r} \in \Lambda^*$ , and that over  $\Lambda^*$  the functions  $\Phi(\mathbf{r})$  and  $g(\mathbf{r})$  are equivalent. This means that reciprocal structures  $\Psi^*$  are equivalent in these two cases.

Hence we claim that it is possible to compute the reciprocal structure for a union of cosets sampling structure by computing the Fourier transform of the signal  $\phi(\mathbf{x})$  defined in equation (2.25).

## 2.5 Reciprocal Structure of Irregular Sampling Structure

In this section, we compute reciprocal structure of a finite irregular sampling structure. A finite irregular sampling structure is a sampling structure which has finite number of irregularly-distributed sample points. Since each pixel in a finite irregular sampling structure is irregularly distributed, each pixel needs to be described by a coset in an orthonormal lattice. So the number of cosets required to describe the structure is equal to the number of sampling points in the sampling structure.

Let us define a finite orthonormal sampling structure  $\varphi$  of dimension  $M \times N$  such that  $\varphi \in \Gamma$ ,  $\Gamma$  being an orthonormal lattice. We define a sampling structure  $\Upsilon$  with  $P$  sample points irregularly-distributed over the orthonormal sampling structure  $\varphi$ . Let us consider a sublattice  $\Lambda$  of  $\Gamma$  which is  $MN$  times sparser than lattice  $\Gamma$ . We can describe a sampling structure  $\Psi$ , such that  $\Upsilon \in \Psi$ , as a union of selected  $P$  cosets of sublattice  $\Lambda$  in lattice  $\Gamma$ .

$$\Psi = \bigcup_{i=1}^P (\mathbf{c}_i + \Lambda) \quad (2.40)$$

We define a signal

$$\phi(\mathbf{x}) = \begin{cases} 1, & \text{for } \mathbf{x} \in \Psi \\ 0, & \text{for } \mathbf{x} \notin \Psi, \mathbf{x} \in \Gamma \end{cases} \quad (2.41)$$

We observe that this signal is the same as the signal for unions of cosets case and hence the results would be also valid for unions of cosets would be valid for this case also. We

use the results of unions of cosets from previous section (eq. 2.37):

$$\Psi^* = \{\mathbf{r}; \Phi(\mathbf{r}) \neq 0, \mathbf{r} = (\mathbf{V}^{-1})^T \mathbf{k}, \mathbf{k} \in Z^N\} \quad (2.42)$$

Since  $\Upsilon \in \Psi$ , the reciprocal structure of  $\Psi$  is the same as the reciprocal structure  $\Upsilon$  as location of sample points outside of  $\varphi$  is of no consequence. The reciprocal structure of  $\Upsilon$  for all practical purposes is same as  $\Psi$ . Hence,

$$\Upsilon^* = \{\mathbf{r}; \Phi(\mathbf{r}) \neq 0, \mathbf{r} = (\mathbf{V}^{-1})^T \mathbf{k}, \mathbf{k} \in Z^N\} \quad (2.43)$$

## 2.6 Using the Fourier transform for Computing Reciprocal Lattice Structure

In this section, we will use some examples to validate the results proposed in this chapter. We take four different sampling structures and demonstrate the validity of the results. Let  $\Psi$  be the sampling structure of which we want to compute reciprocal sampling structure. We generate a matrix which contains either 1 or 0 for all sample points. The elements of matrix which belong to  $\Psi$  are assigned value of 1 and all other elements of matrix are assigned zero value. We then compute the discrete Fourier transform (DFT) of the matrix. The resulting matrix gives us reciprocal sampling structure  $\Psi^*$ . An element of matrix belongs to the reciprocal structure if it is not zero. Using this method, we compute the reciprocal structure for four different cases.

(a) Orthogonal lattice: Let us define the underlying orthonormal lattice  $\Gamma$  with the sampling matrix as follows:

$$V_{\Gamma} = \begin{pmatrix} 1 & 0 \\ 0 & 1 \end{pmatrix} \quad (2.44)$$

and let  $\Lambda$  be the orthogonal lattice with the sampling matrix given below:

$$V_{\Lambda} = \begin{pmatrix} 2 & 0 \\ 0 & 1 \end{pmatrix} \quad (2.45)$$

Fig. 2·1 (a) shows lattices  $\Gamma$  and  $\Lambda$ . Fig. 2·1 (b) shows reciprocal lattice  $\Lambda^*$  and the associated Voronoi diagram. A Voronoi diagram is a diagram in which every point  $\mathbf{x} \in R^N$  is assigned to its nearest neighborhood point  $\mathbf{y} \in \Psi^*$  (Aurenhammer, 1991). A Voronoi cell associated with point  $\mathbf{y}$  can be defined as:

$$V(\mathbf{y}) = \{\mathbf{x} : |\mathbf{x} - \mathbf{y}| \leq |\mathbf{x} - \mathbf{k}|, \text{ for all } \mathbf{k} \in \Psi^* \setminus \mathbf{y}\} \quad (2.46)$$

A Voronoi diagram is sometimes also known as nearest-neighbor diagram. A Voronoi cell associated with vector  $\mathbf{0}$  is a special Voronoi cell in the sense that it tells us how spectrum should be confined in order to avoid aliasing. A Voronoi cell associated with vector  $\mathbf{0}$  is also known as the Nyquist area.

(b) Nonorthogonal lattice: Let  $\Lambda$  be a non-orthogonal lattice with the sampling matrix given below:

$$V_{\Lambda} = \begin{pmatrix} 0 & 2 \\ 2 & 1 \end{pmatrix} \quad (2.47)$$

The Fig. 2·2 (a) shows lattices  $\Gamma$  and  $\Lambda$ . Fig. 2·2 (b) shows reciprocal lattice  $\Lambda^*$  and the associated Voronoi diagram.

(c) Union of cosets: Let  $\Psi$  be the union of cosets of lattice  $\Lambda$  in lattice  $\Gamma$ .

$$\Psi = \Lambda \cup (c + \Lambda) \quad (2.48)$$

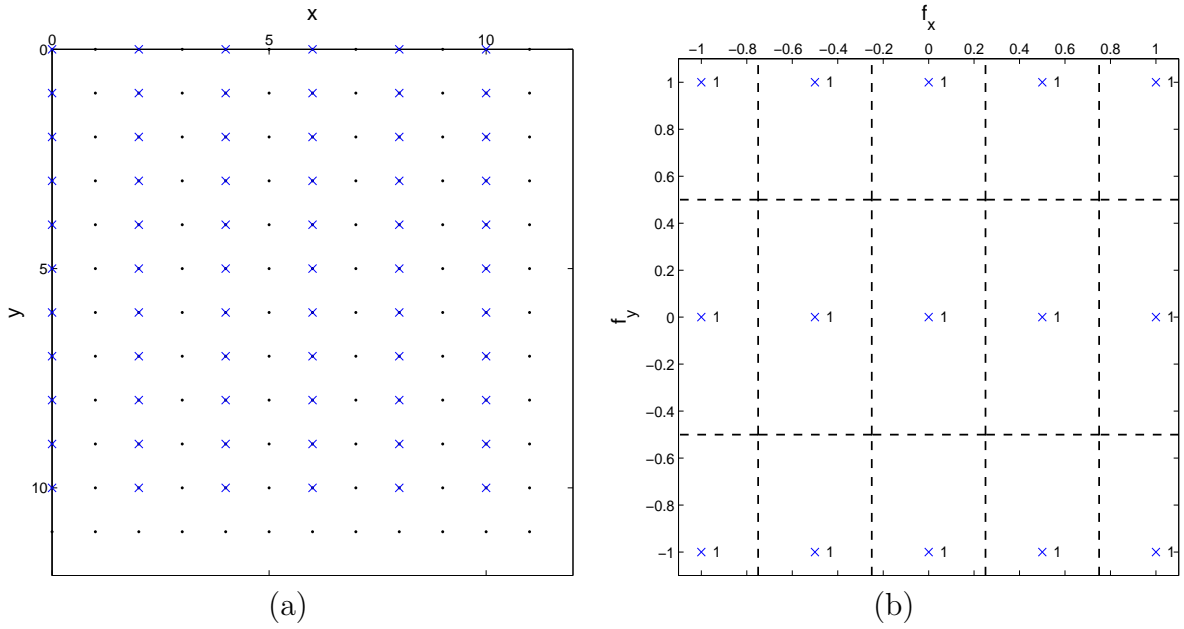


**Figure 2-1:** (a) Orthogonal lattice  $\Lambda$  ( $\times$ ) along with the underlying orthonormal lattice  $\Gamma$  ( $\cdot$ ), (b) reciprocal structure  $\Lambda^*$  ( $\times$ ) to the orthogonal lattice.

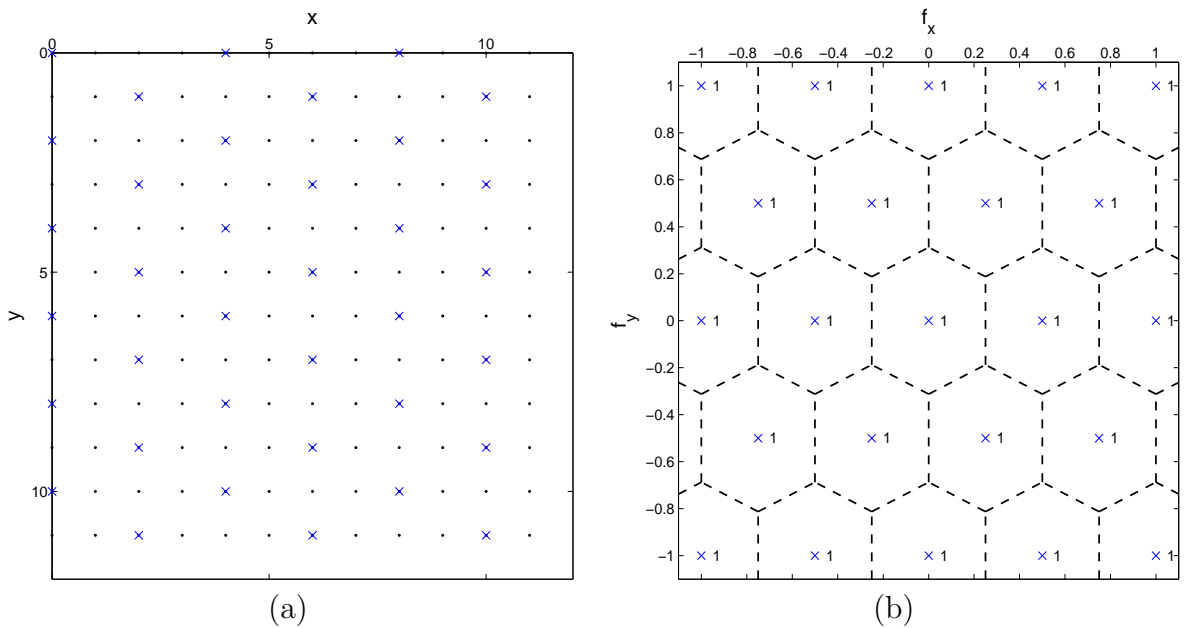


**Figure 2-2:** (a) Non-orthogonal lattice  $\Lambda$  ( $\times$ ) along with underlying orthonormal lattice  $\Gamma$  ( $\cdot$ ), (b) reciprocal structure  $\Lambda^*$  ( $\times$ ) to the non-orthogonal lattice.

with the sampling matrix of  $\Lambda$  given below:

$$V_{\Lambda} = \begin{pmatrix} 0 & 2 \\ 2 & 1 \end{pmatrix} \quad (2.49)$$

$$c = \begin{pmatrix} 1 \\ 0 \end{pmatrix} \quad (2.50)$$

The Fig. 2-3 (a) shows lattices  $\Gamma$  and unions of cosets  $\Psi$ . Fig. 2-3 (b) shows reciprocal sampling  $\Psi^*$  and the associated Voronoi diagram.

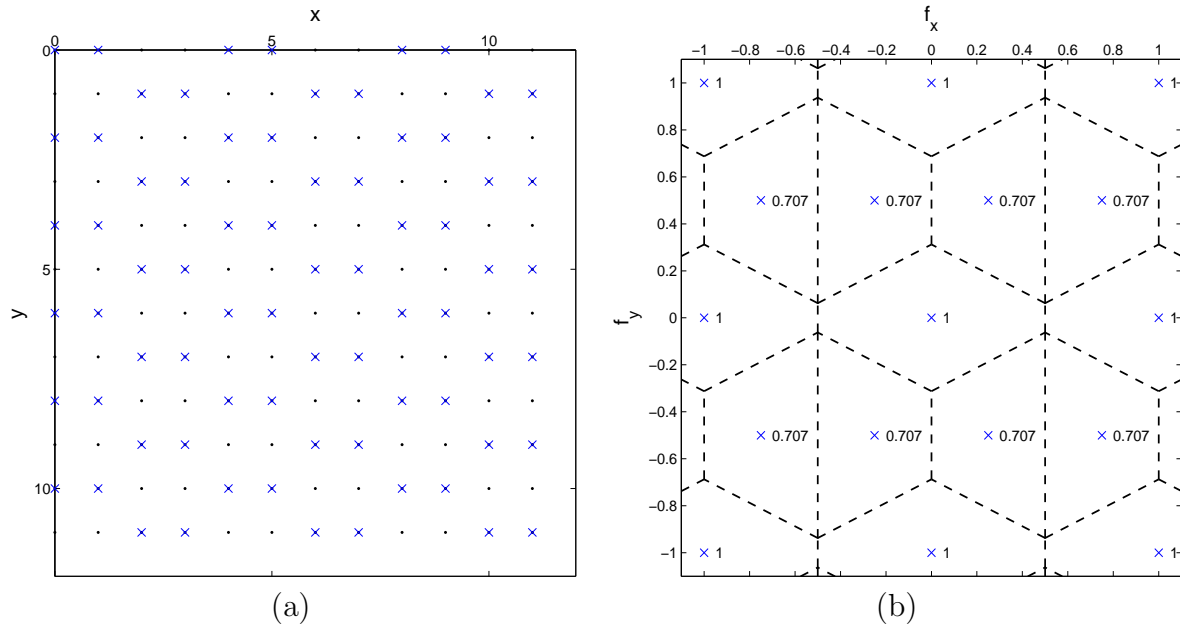


**Figure 2-3:** (a) Union of cosets  $\Psi$  ( $\times$ ) along with the underlying orthonormal lattice  $\Gamma$  ( $\cdot$ ), (b) reciprocal structure  $\Psi^*$  ( $\times$ ) to the union of cosets sampling structure.

d) Random Sampling: A random sampling structure  $\Psi$  is defined with respect to the orthonormal sampling structure  $\Gamma$ . The sample points are irregular and cannot be

defined using a union of cosets. The sample points were randomly generated. The reciprocal structure of  $\Psi$  is computed using 2D Fourier transform. The results were thresholded using 0.2 as the threshold for visual clarity. The Fig. 2·4 (a) shows lattices  $\Gamma$  and sampling structure  $\Psi$ . Fig. 2·4 (b) shows reciprocal sampling structure  $\Psi^*$  and the associated Voronoi diagram.

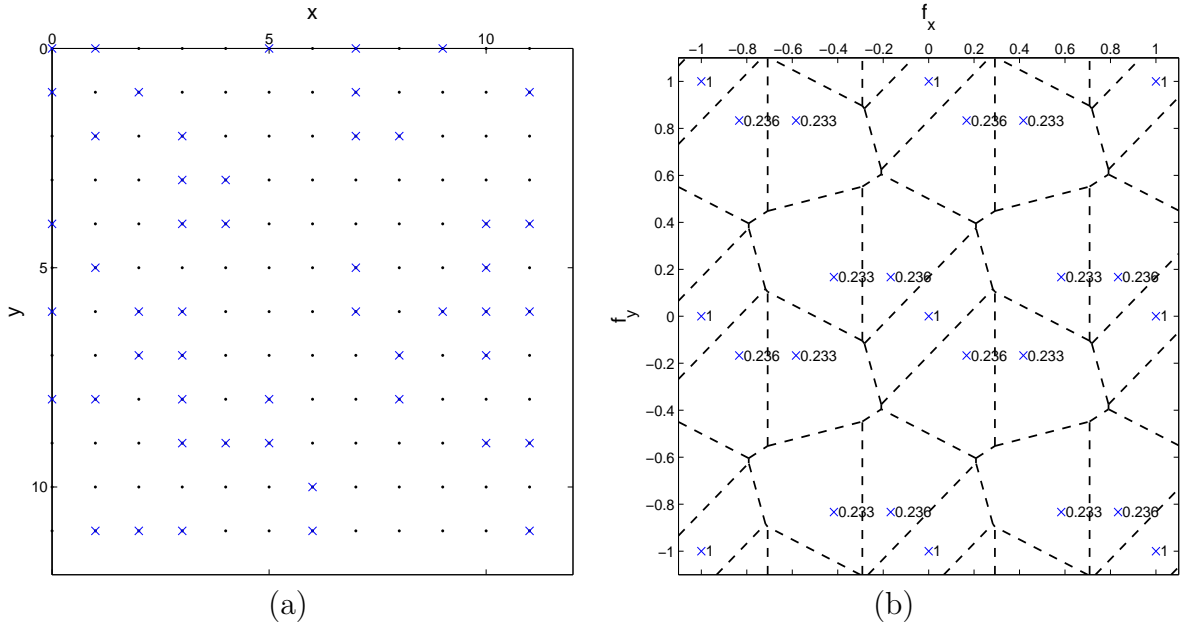


**Figure 2·4:** (a) Random sampling structure  $\Psi$  ( $\times$ ) along with underlying orthogonal lattice  $\Gamma$  ( $\cdot$ ), (b) Reciprocal structure  $\Psi^*$  ( $\times$ ) to the random sampling structure.

The results obtained for all examples would be the same had they been computed using the methods proposed by Dubois (Dubois, 1985). In the last example, the results obtained would be the same if we were to model it as a union of cosets and each coset would contain just one sample point. The results in this chapter show that a reciprocal structure for any sampling structure can be computed efficiently by applying discrete space Fourier transform to signal  $\phi(\mathbf{x})$ , which is 1 at points which belong to the sampling structure and zero elsewhere.



## Chapter 3

# Crosstalk-Aware Sampling Structure

### 3.1 Sampling Model for Automultiscopic Displays

Automultiscopic displays simulate the binocular disparity depth cue by projecting distinct image to each eye. The views are multiplexed in such a way that left and right views of the scene are projected on the left and right eyes, respectively. This stereo pair of images allows human visual system to perceive depth, an important cue for 3-D visualization.

The automultiscopic displays available on the market suffer from crosstalk between views. This means that a portion of left view of a scene is visible to the right eye with reduced intensity and vice versa (Klimenko et al., 2003a). As a result, the user observes ghost images at object boundaries which interferes with 3-D perception of the image (Konrad et al., 2000). The presence of crosstalk, in automultiscopic displays, increases the perceived resolution of the image as shown in Fig 3-1 as compared to the case without crosstalk in Fig 3-2. The image with crosstalk seems to be of better quality and contains a lot more details as claimed by Berkel (Berkel and Clarke, 1997). The increase in perceived resolution of the image should be taken into account while designing anti alias filters for the subsampling operation.



(a)

**Figure 3.1:** Image with crosstalk from other views. Number of views = 4. crosstalk coefficient = 0.5



(a)

**Figure 3-2:** Image with no crosstalk from other views. Number of views = 4.

## 3.2 Perceived Sampling

As discussed in the previous section, there is an increase in perceived resolution of the image due to crosstalk. This increase should be taken into account in designing the antialiasing filters using subsampling operation. The effect of increased perceived resolution can be incorporated into the design of antialias filters by modeling the crosstalk present in the displays. In this section, we develop mathematical foundation of perceived sampling and analyze its effect on frequency of support. For a given sampling structure, we define its frequency of support as a range of frequencies which do not undergo any aliasing during sampling of a signal. Though all our discussion will be limited to 1-D sampling, the results are also valid for 2-D sampling of images.

The subsampling of a 1-D discrete-time signal can be considered to be the multiplication of a discrete signal with a train of Kronecker delta impulses. This can be considered as normal subsampling operation without taking into account any crosstalk effect. To incorporate crosstalk into our model, we would have to include an impulse function with magnitude equal to the crosstalk coefficient. The train of sampling impulses for both sampling without crosstalk and with crosstalk are shown in Fig 3-3.

In the subsequent mathematical model, we assume that our display has  $N$  views and that there is subsampling only in horizontal direction. The views are at regular interval in space and there is no crosstalk between the views.

The subsampling pattern (train of impulses that multiplies the discrete signal) for each view without considering crosstalk can be mathematically expressed as follows:

$$x(t) = \sum_{n=-\infty}^{+\infty} \delta(t - nN), \text{ for } t \in Z \quad (3.1)$$

where,  $N$  is the time or physical spacing between two adjacent pixels/Kronecker impulses in one view.

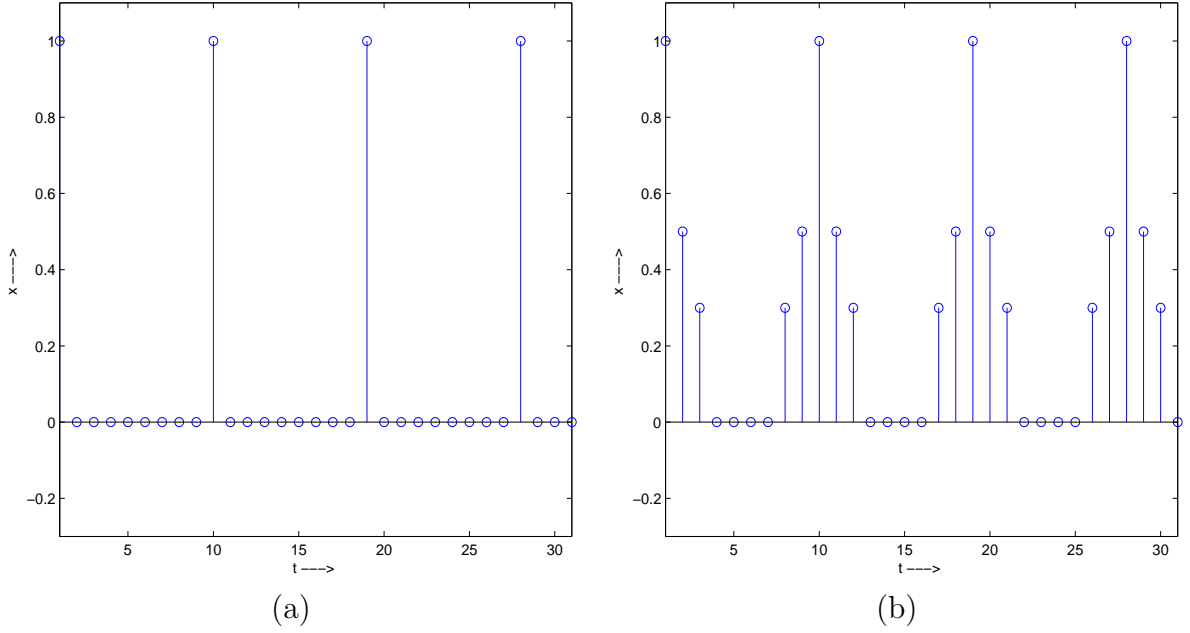


**Figure 3.3:** (a) Sampling pattern without crosstalk (b) Sampling pattern with crosstalk

The Fourier transform of the above train of unit impulses is:

$$X(\omega) = \frac{2\pi}{N} \sum_{n=-\infty}^{+\infty} \delta\left(\omega - \frac{2\pi}{N}n\right) \quad (3.2)$$

This can be also written as:

$$X(f) = \frac{1}{N} \sum_{n=-\infty}^{+\infty} \delta\left(f - \frac{1}{N}n\right) \quad (3.3)$$

In this case, the discrete signal can represent frequencies up to  $\frac{1}{2N}$  without any aliasing and we would need to filter any frequencies greater than  $\frac{1}{2N}$  before subsampling.

Now we consider the case in which display suffers from crosstalk between the views. If we assume  $N$  views in our monitor,  $N$  being odd, then we have crosstalk from  $M = (N + 1)/2$  views from each side. The perceived sampling in this case can be represented as the sum of impulse trains with different amplitudes and phase shifts.

Given below are mathematical expressions of sampling for each of the views. As-

suming view  $M$  is intended, the crosstalk coefficients between the intended view  $M$  and views  $M + 1, M + 2, \dots, 2M - 1$  are  $a_1, a_2, \dots, a_{M-1}$ , respectively. Assuming the crosstalk into the intended view from spatially symmetric views to be equal, the crosstalk coefficients between the intended view  $M$  and views  $M - 1, M - 2, \dots, 1$  are  $a_1, a_2, \dots, a_{M-1}$ , respectively. It is assumed that the intended view is seen at full brightness implying that  $a_0$  is equal to 1. The values of crosstalk coefficients  $a_i$  lie between 0 and 1.

View  $M$  (intended view) is seen at full brightness:

$$x_M(t) = \sum_{n=-\infty}^{+\infty} \delta(t - nN) \quad (3.4)$$

Crosstalk from view  $M + 1$  has gain of  $a_1$ :

$$x_{M+1}(t) = a_1 \sum_{n=-\infty}^{+\infty} \delta(t - nN + 1) \quad (3.5)$$

Crosstalk from view  $M - 1$  has gain of  $a_1$ :

$$x_{M-1}(t) = a_1 \sum_{n=-\infty}^{+\infty} \delta(t - nN - 1) \quad (3.6)$$

.

.

.

Crosstalk from view  $2M - 1$  has gain of  $a_{M-1}$ :

$$x_{2M-1}(t) = a_{M-1} \sum_{n=-\infty}^{+\infty} \delta(t - nN + M - 1) \quad (3.7)$$

Crosstalk from view 1 has gain of  $a_{M-1}$ :

$$x_1(t) = a_{M-1} \sum_{n=-\infty}^{+\infty} \delta(t - nN - M + 1) \quad (3.8)$$

The contribution of all pixels to the perception of the intended view can be modeled as sampling of full image by the following train of impulses.

$$x_{net}(t) = x_1(t) + x_2(t) + \dots + x_{2M-1}(t) \quad (3.9)$$

The Fourier transform of  $x_{net}(t)$  can be written as:

$$X(f) = \frac{1}{N} \sum_{n=-\infty}^{+\infty} \delta\left(f - \frac{n}{N}\right) [1 + 2a_1 \cos(2\pi f) + 2a_2 \cos(4\pi f) + \dots + 2a_{M-1} \cos((M-1)2\pi f)] \quad (3.10)$$

For  $f = 0$ , all the components are in phase:

$$X(f) = \frac{1}{N} [1 + 2a_1 + 2a_2 + \dots + 2a_{M-1}] \quad (3.11)$$

At  $f = \frac{1}{N}$ , we have

$$X(f) = \frac{1}{N} [1 + 2a_1 \cos\left(\frac{2\pi}{N}\right) + 2a_2 \cos\left(\frac{4\pi}{N}\right) + \dots + 2a_{M-1} \cos\left((M-1)\frac{2\pi}{N}\right)] \quad (3.12)$$

Now, we have the original signal at  $f = 0$  and nearest alias at  $f = \pm \frac{1}{N}$ . The original signal at  $f = 0$  has greater energy than the nearest aliases and this would allow us to relax the filter bandwidth to a greater degree than  $\frac{1}{N}$  before subsampling. The exact filter bandwidth would depend on the number of views  $N$  in the display.

We will present an example of automultiscopic display with  $N = 3$  views. The value of  $M$  is 2 in this case. The crosstalk coefficient  $a_1$  is 0.6285. The comparison of the original signal energy for display with and without crosstalk is shown in Fig 3-4. The nearest alias component, in case of no crosstalk, has the same energy as the original

signal. In the case with crosstalk, the signal energy of alias signal is less than the original signal energy by approximately 84 percent.

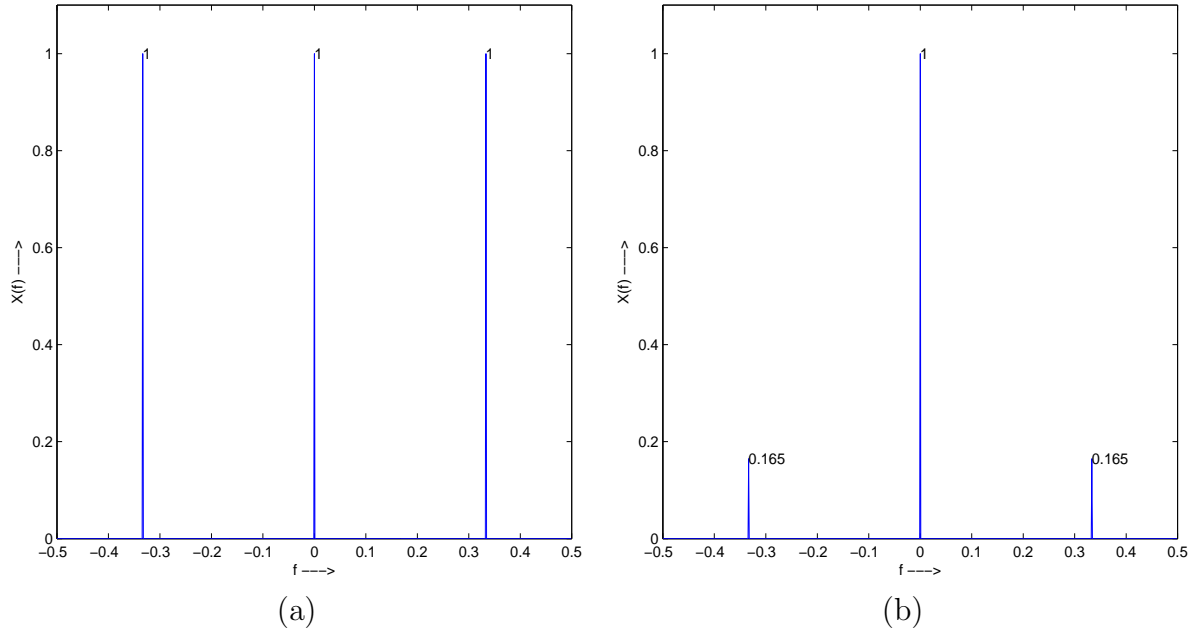


**Figure 3-4:** Original and nearest alias signal energy: (a) without crosstalk (b) with crosstalk ( $N = 3$ )

### 3.3 Computing Filter Bandwidth Using Image Covariance Models

In the normal subsampling case, the aliasing signal has the same energy as the original signal. So it is easy to compute the ideal antialias filter bandwidth which is exactly mid-way between the original signal center frequency and alias signal center frequency. However, in the case of crosstalk the energy in the alias signal is different from the original signal energy. To compute the filter bandwidth in this case, we need to make some reasonable assumptions about image properties. We will use a covariance model to statistically approximate the actual image data.

The covariance model is based on the assumption that the closer the pixels are in an

image, the more correlated they are. It is possible to use exponential autocorrelation models to model natural and computer-generated images quite precisely.

The separable exponential autocorrelation model can be expressed mathematically as follows:

$$R_u[m_1, m_2] = \rho_1^{|m_1|} \rho_2^{|m_2|} \quad (3.13)$$

Since the model is separable, the one dimensional equivalent of the above equation can be written as:

$$R_u[m] = \rho_1^{|m|} \quad (3.14)$$

The Fourier transform of exponential function is:

$$F\{e^{-2\pi f_0|x|}\}(f) = \frac{1}{\pi} \frac{f_0}{f^2 + f_0^2} \quad (3.15)$$

Using equations (3.14) and (3.15), we compute the power spectral density, which is the Fourier transform of auto correlation  $R_u$ , of the image:

$$F\{\rho_1^{|m|}\}(f) = \frac{1}{\pi} \frac{f_0}{f^2 + f_0^2} \quad (3.16)$$

where  $f_0 = \frac{-1}{2\pi} \ln(\rho_1)$ .

We are sampling a 1-D signal with power density spectrum given in equation (3.16). This signal is sampled by a train of impulse functions with frequency spectrum such as one shown in Fig. 3-4(b). As sampling of a signal in time domain is a multiplication operation, it results in a convolution operation in frequency domain. This leads to copies of Fourier transform centered at  $f = 0, \pm \frac{n}{N}, n \in Z$ . The mathematical expression of Fourier transform centered at  $f = 0$  is  $\frac{f_0}{f^2 + f_0^2}$ . Similarly a copy of Fourier transform centered at  $f = 1/N$  is  $\frac{Af_0}{(1/N - f)^2 + f_0^2}$ , where  $A$  is a gain factor defined as the ratio of nearest alias signal energy to the original signal energy. We can define  $A$  mathematically

as:

$$A = \frac{X(f)_{f=\frac{1}{N}}}{X(f)_{f=0}} \quad (3.17)$$

Using this information we find the filter cutoff frequency.

In order to minimize aliasing from repeat spectra while maximally preserving spectral content of the original signal, we propose to define the cut-off frequency  $f_c$  of the filter as a frequency for which the repeat spectrum equals the original spectrum, expressed as follows:

$$\frac{f_0}{f^2 + f_0^2} = \frac{Af_0}{(\frac{1}{N} - f_c)^2 + f_0^2} \quad (3.18)$$

Solving the above equation, we get the following cut off frequency,

$$f_c = \begin{cases} \frac{+(\frac{2}{N}) \pm \sqrt{(\frac{2}{N})^2 - 4\{1-A\}\{(\frac{1}{N})^2 + f_0^2 - Af_0^2\}}}{2(1-A)}, & \text{for } A \neq 1 \\ \frac{1}{N}, & \text{for } A = 1 \end{cases} \quad (3.19)$$

where  $f_0 = \frac{-1}{2\pi} \ln(\rho_1)$ .

If we substitute  $A = 1$ , then the above bandwidth of filter would reduce to the no-crosstalk case. Another observation is that  $A$  is always less than 1 which means the bandwidth of filter for displays with crosstalk will always be greater than for those with no crosstalk. This would allow us to relax the bandwidth of antialiasing filter.

Let us demonstrate this by an example. Assume  $N = 3$  views and let us choose our  $\rho_1 = 0.9$  and  $a_1 = 0.6285$ . For this specification, we would have

$$A = 0.165, f_0 = 0.0168 \quad (3.20)$$

The frequency-domain representation of signal for no-crosstalk and crosstalk case is shown in Fig 3-5. Solving the above equations for antialias filter cut-off frequency we

get  $f_c = 1/1.78$  which is significantly larger than  $1/3$ . This validates our argument that crosstalk aware anti-alias filter would be less restrictive.

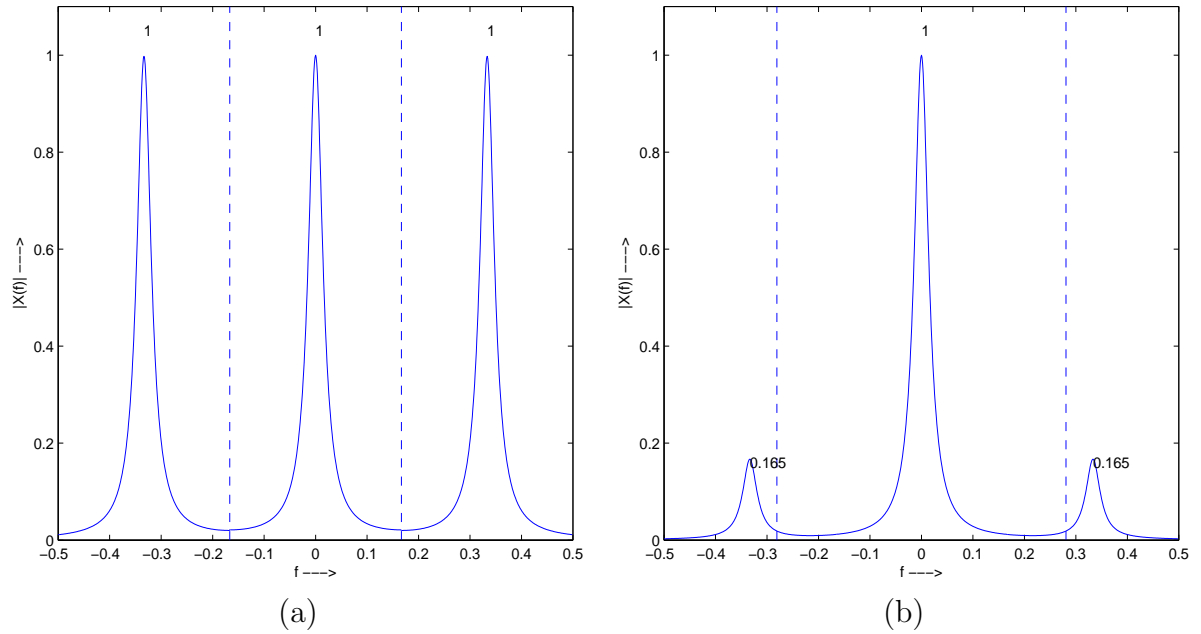


**Figure 3-5:** Original and nearest alias signal energy: (a) without crosstalk, filter bandwidth = 0.33 (b) with crosstalk, filter bandwidth = 0.56



## Chapter 4

# Design of Anti-alias Filters

In this chapter, we discuss the measurement of crosstalk between views for Synthgram SG202 lenticular display. We use these crosstalk measurements and sampling structures of individual views to generate the perceived sampling structure and its corresponding reciprocal sampling structure. Due to crosstalk from other views, an observer is able to see some pixels which do not belong to the intended view. If we include these extra pixels in our sampling structure; this new modified structure is termed as a “perceived” sampling structure. Using this reciprocal sampling structure along with the image covariance model, we compute the frequency response of desired anti-alias filter. We then proceed to design a two-dimensional anti-alias filter matching the desired frequency response. We use the anti-alias filter to filter the individual views before interzigging them. In the end, we present and discuss the results of using anti-alias filter on interzigged 3-D images.

### 4.1 Measurement of Crosstalk

In this section, we describe and present the results of measurement of crosstalk in Synthgram SG202 lenticular automultiscopic display. The resolution of this LCD display is  $1600 \times 1200$  pixels. In this display, we have nine views each of which provides a different perspective of a scene to the viewer. Each view has been assigned an approximately equal number of pixels from the total of  $1600 \times 1200$  pixels. The pixel assignment to each view is quite irregular in space (Agniel, 2004). This is a desired property in lentic-

ular displays because it reduces the *Moiré* effect, and has been achieved by slanting the lenticular sheet at a small angle. However this irregular pixel mapping makes the task of designing an appropriate anti-alias filter difficult.

In these monitors, even though a viewer is supposed to view a pair of intended views from the total of 9 views, there is some leakage of light from neighboring views. This modifies the visual experience of the viewer and in this section we make an effort to quantify the amount of crosstalk between two views.

We used a digital camera to measure the amount of light emitted by our SG202 display. Since we measure a range of intensities using this camera, an experiment was conducted first to establish linearity of the setup and of the measuring instruments. The following are the steps of experiment conducted to verify the linearity of the camera:

1. In the first step, view number 1 was illuminated using white image (maximum brightness of 255) and a camera was placed in such a way that it received the maximum amount of light. The process of identifying the right location of camera was done manually.
2. Once the location of the camera was fixed, the intensity with which the intended view was illuminated was varied from 0 to 255. The amount of light captured by the camera was measured for different levels of displayed intensities.
3. The plot of actual display intensity versus the received intensity is shown in Fig 4.1.

From the plot in Fig. 4.1, we can assume that our setup to measure the crosstalk was reasonably linear except at the extreme end of the image intensity range.

We now describe the experiment to measure the crosstalk of the Synthagram lenticular automultiscopic display SG202 using the same digital camera. The steps of experiment are described below:

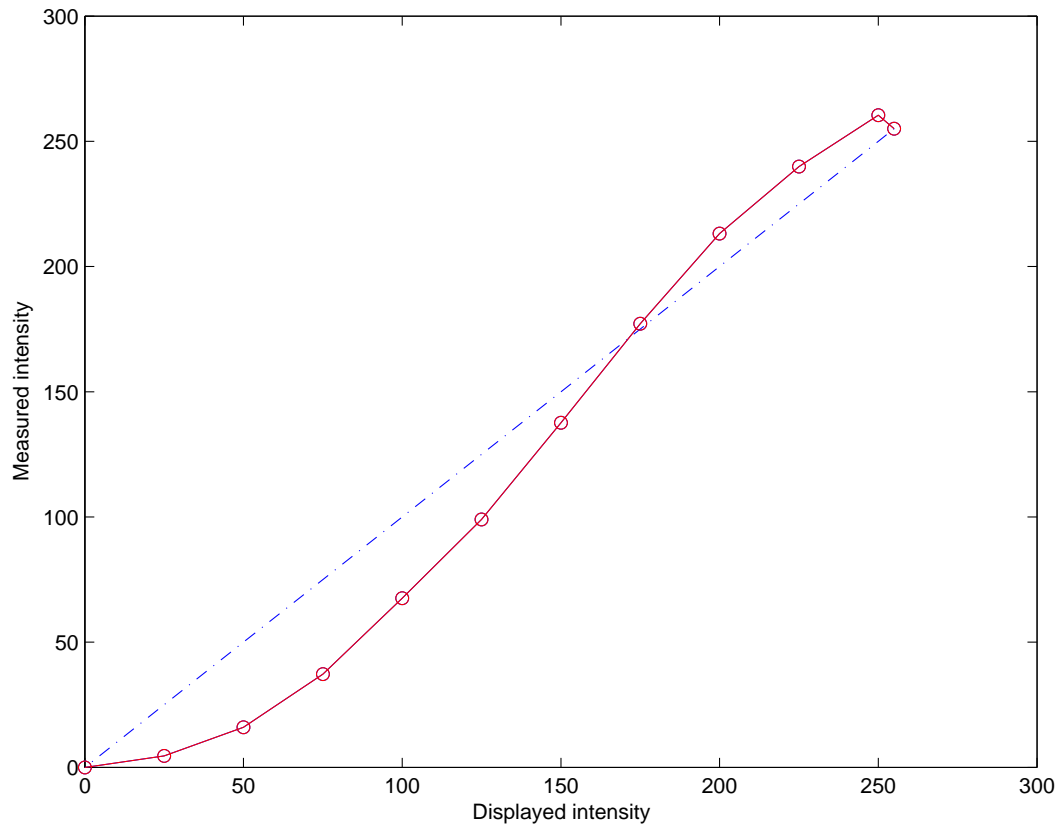


**Figure 4.1:** Measurement of camera linearity characteristics

1. Initially, view number 3 was displayed using a white image and the camera was placed where it received the maximum amount of light. The process of identifying the correct location of camera was done manually.
2. Once the location of the camera was fixed, all the views from view 1 to view 9 were illuminated and images of the display screen were captured with the camera. These images were used to estimate the amount of light intensity captured by the camera.
3. The above steps were repeated with the camera placed to capture different views.

All the above steps were performed in a darkroom where no other source of light was present. The camera was in manual mode to keep aperture and focal length constant during the measurement. The advantage of measuring the crosstalk using this method is that it allows us to measure the spatial variation in crosstalk. Also it allows us to measure crosstalk for each color; red, green, and blue simultaneously. The monitor used for this experiment was the Synthagram SG202. Also an image of display without any view being illuminated was captured to create a black reference for the crosstalk calculation.

The crosstalk measurement results are shown in Tables 4.1 and 4.2.

<i>View No. →</i>	<i>1</i>	<i>2</i>	<i>3</i>	<i>4</i>	<i>5</i>	<i>6</i>	<i>7</i>	<i>8</i>	<i>9</i>
<i>Crosstalk ratio: R</i>	<i>1.0</i>	<i>0.628</i>	<i>0.128</i>	<i>0.010</i>	<i>0.004</i>	<i>0.004</i>	<i>0.010</i>	<i>0.117</i>	<i>0.589</i>
<i>Crosstalk ratio: G</i>	<i>1.0</i>	<i>0.665</i>	<i>0.159</i>	<i>0.015</i>	<i>0.005</i>	<i>0.005</i>	<i>0.014</i>	<i>0.132</i>	<i>0.596</i>
<i>Crosstalk ratio: B</i>	<i>1.0</i>	<i>0.683</i>	<i>0.173</i>	<i>0.016</i>	<i>0.004</i>	<i>0.004</i>	<i>0.013</i>	<i>0.134</i>	<i>0.596</i>
<i>Crosstalk ratio: Y</i>	<i>1.0</i>	<i>0.656</i>	<i>0.151</i>	<i>0.014</i>	<i>0.004</i>	<i>0.004</i>	<i>0.012</i>	<i>0.127</i>	<i>0.594</i>

**Table 4.1:** Crosstalk measurements with view 1 as center

From the above table of crosstalk measurements, we can make the following inferences:

<i>View No. →</i>	<i>1</i>	<i>2</i>	<i>3</i>	<i>4</i>	<i>5</i>	<i>6</i>	<i>7</i>	<i>8</i>	<i>9</i>
<i>Crosstalk ratio: R</i>	<i>0.093</i>	<i>0.598</i>	<i>1.000</i>	<i>0.640</i>	<i>0.143</i>	<i>0.013</i>	<i>0.006</i>	<i>0.006</i>	<i>0.011</i>
<i>Crosstalk ratio: G</i>	<i>0.112</i>	<i>0.608</i>	<i>1.000</i>	<i>0.667</i>	<i>0.172</i>	<i>0.017</i>	<i>0.005</i>	<i>0.005</i>	<i>0.012</i>
<i>Crosstalk ratio: B</i>	<i>0.114</i>	<i>0.618</i>	<i>1.000</i>	<i>0.678</i>	<i>0.186</i>	<i>0.017</i>	<i>0.004</i>	<i>0.004</i>	<i>0.012</i>
<i>Crosstalk ratio: Y</i>	<i>0.106</i>	<i>0.605</i>	<i>1.000</i>	<i>0.660</i>	<i>0.164</i>	<i>0.015</i>	<i>0.005</i>	<i>0.004</i>	<i>0.011</i>

**Table 4.2:** Crosstalk measurements with view 3 as center.

1. The amount of crosstalk for the three primary colors (red, green and blue) were approximately equal. So we can just design our filter for one color and apply it for other colors too.
2. The crosstalk is more or less spatially symmetric. The crosstalk from view 2 and view 9 into view 1 is approximately the same. A Similar observation holds for views 3 and 8, views 4 and 7, views 5 and 6.
3. The crosstalk for any view is a function of distance between them. For example, view 1 and view 2 have the same crosstalk level as view 3 and view 4. Similarly, crosstalk between view 1 and view 3 has the same crosstalk level as that between view 3 and 5. This spatial invariance of crosstalk allows us to design a common anti-alias filter for one view and use it for other views.

## 4.2 Perceived Sampling Structure

Using the crosstalk measurements given in the previous section and sampling structure for individual views, we can create a perceived sampling structure for each individual view of display SG202.

Fig 4-2(a) shows the pixel assignment of view 1. Since we know the amount of crosstalk between the views, we can use the information to construct a perceived sampling structure for view 1. Fig 4-2(b) shows the perceived sampling structure of view 1. In Fig. 4-2(b), the set of pixels with crosstalk ratio less than 0.1 has been ignored for

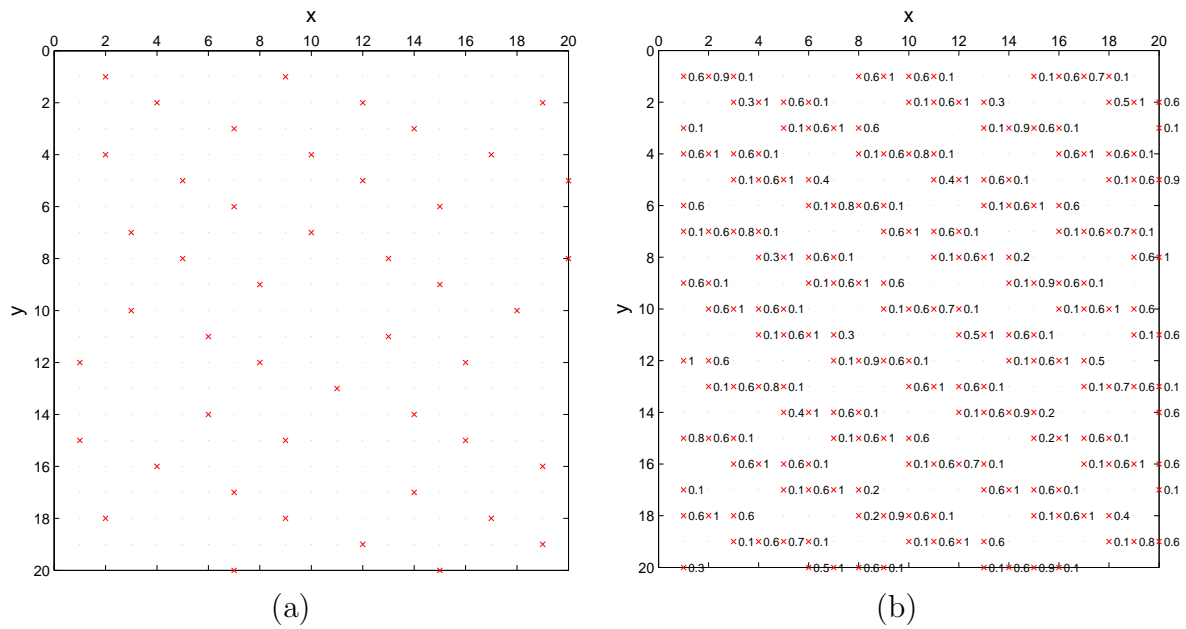


**Figure 4.2:** (a) Sampling structure of red color component of view 1, (b) Perceived sampling structure of red color component of view 1 (For the sake of visual clarity, only neighboring-view samples with crosstalk ratio of 0.1 or more are shown).

clarity.

The sampling structure in Fig. 4.2(a) shows us that we have a downsampling by factor of 9 if these pixels were periodic in nature. The sampling structure in Fig. 4.2(b) shows us that we have a downsampling by factor of 3.61 if these pixels were periodic in nature. Though none of the sampling structures are periodic, it gives us an intuitive idea that including crosstalk in our model would change the filter bandwidth of our anti-alias filter significantly.

### 4.3 Computing Reciprocal Structure

We now use the method proposed in Chapter 2 to compute the reciprocal sampling structure for the sampling structures shown in Fig. 4.2.

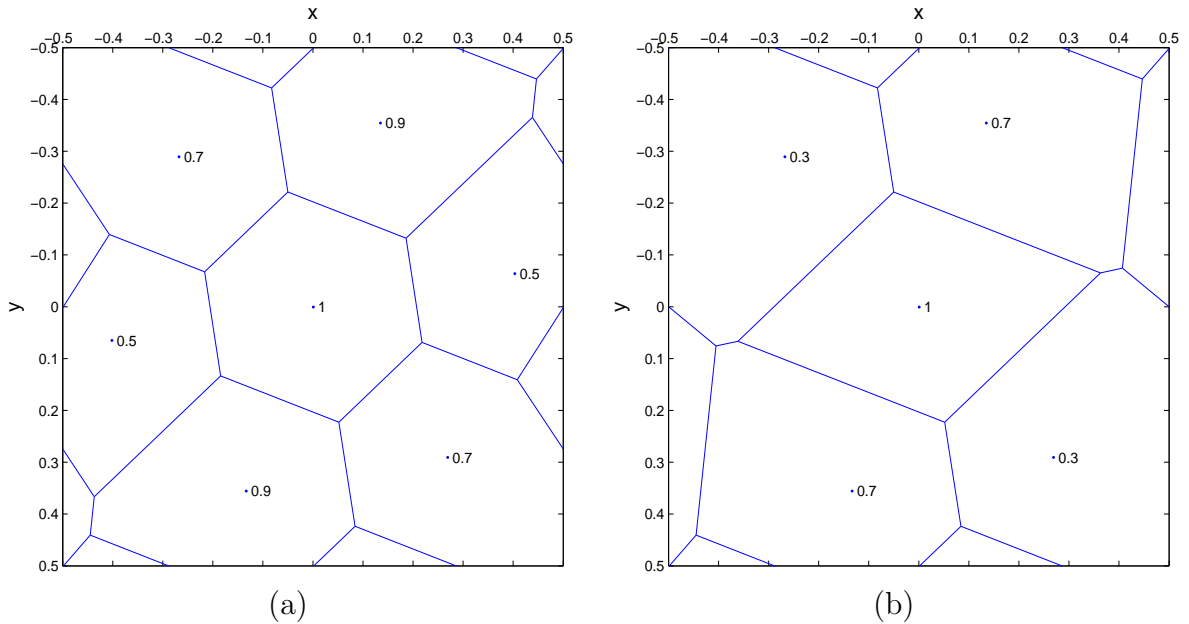


**Figure 4.3:** (a) Reciprocal sampling structure, (b) Reciprocal crosstalk-aware sampling structure (For the sake of visual clarity, only locations of spectral replications with the gain of 0.2 or more are used to compute the Voronoi diagram and shown).

We create a 2-D discrete space signal  $\Phi(\mathbf{x})$  of dimension  $1600 \times 1200$ , the sample

values of points corresponding to view 1 are assigned 1. All other sample values of the signal are set to zero. We can compute the reciprocal sampling structure by computing 2-D Fourier transform of the signal  $\Phi(\mathbf{x})$ . Fig. 4-3 (a) shows the reciprocal structure corresponding to sampling structure in Fig. 4-2(a). Similarly, Fig. 4-3(b) shows the reciprocal structure corresponding to sampling structure in Fig. 4-2(b). In both the cases, sample values lower than 0.2 have been removed to assure visual clarity in the figure.

However, in this case we can make reasonable assumptions about the signal spectrum and can design filters in a more accurate manner. The knowledge of the frequency spectrum of the signal allows us to exploit the fact that gain factors associated with alias signals are less than 1. We use the image covariance model, discussed in chapter 3, to approximate the spectrum of the image. The image covariance model of equation (3.13) can be written as follows:

$$R_u[m_1, m_2] = \rho_1^{|m_1|} \rho_2^{|m_2|} \quad (4.1)$$

The corresponding power spectrum density is:

$$\Phi(f_x, f_y) = \frac{1}{\pi^2} \frac{f_0^2}{(f_x^2 + f_0^2)(f_y^2 + f_0^2)} \quad (4.2)$$

Each point in the reciprocal sampling structure (Fig. 4-3) has a gain factor associated with it. We classify our reciprocal sampling structure gains into three categories:

- Original signal gain: This is a gain associated with the original signal which we want to recover after filtering.
- Alias Signal Energy: These are the gains associated with aliasing signal and have value greater than 0.2.

- Noise Signal Energy: These are the gains associated with noise signals and have value less than 0.2.

Suppose we have signal with the bandwidth of 800Hz and we decide to sample the signal at 1.5 KHz with a periodic sampling structure. The signal energy from frequencies 750-800 Hz will get mapped to 0-50 Hz range after sampling and would cause aliasing. If we perform irregular sampling with average sampling rate of 1.5 KHz, a part of signal energy from frequency 750-800 Hz will be mapped to 0-50 Hz range and would cause aliasing. The remaining part of signal energy would get mapped onto 0-750 Hz range and would appear as noise. In this context, we use the term alias signal energy and noise signal energy.

The classification between the alias signal energy and noise signal energy on the basis of threshold is somewhat arbitrary. However, the effects of these two signals on the image quality are quite different. The effect of alias signals is that of *Moiré* patterns and that of noise signals is grainy nature of the image.

The reciprocal structure contains many points; each point corresponds to replication of the original signal spectra. The point which corresponds to  $\mathbf{0}$  represents the original signal spectrum which we want to recover. All other points correspond to alias or noise signal spectrum. Using the covariance model for image spectrum, we can compute the amount of original signal energy and alias-noise energy at each point in frequency space. Since we would like to maximize the SNR of filtered image, we should define the passband of anti-alias filter as the location where original signal energy is greater than alias-noise signal energy i.e. wherever we have original signal energy greater than the sum of alias and noise signal energy, we have filter magnitude response equal to 1, and 0 elsewhere.

This process gives us the frequency response of the desired filter. We need to design a 2-D filter with the desired frequency response. For this we use the MATLAB function

‘fwind1’ to design a 2-D filter. The function fwind1 designs two-dimensional FIR filters using the window method. In this method, we compute the inverse Fourier transform which gives us the time domain impulse response of the desired filter. But this would give us a large number of filter coefficients. So we truncate the filter coefficients to give us a desired number of filter coefficients. The number of coefficients can be reduced by truncating the time domain impulse response. The truncation can be done using commonly used windows such as the rectangular, Hanning, Hamming, and Blackman. Since the Hamming window gives us the best overall characteristics such as moderate main-lobe width ( $\frac{8\pi}{M}$ ), and moderate side lobe attenuation (-41 dB), we used it for our filter design.

The 2-D filter designed in this case has size of  $51 \times 51$ . The larger the number of coefficients, the better the filter characteristics. We define 2D anti-alias filter passband as follows:

$$H(f) = \begin{cases} 1, & \text{if } E_o > K(E_a + E_n) \\ 0, & \text{otherwise} \end{cases} \quad (4.3)$$

where  $E_o$  is the original signal energy,  $E_a$  is alias signal energy, and  $E_n$  is noise signal energy.

In the above equation, we can change the value of  $K$  to change the passband area of the specified filter. To maximize the signal to noise ratio of the filtered image, we should choose  $K = 1$ . The shaded region in Fig. 4.4 (b) shows the passband region of an ideal anti-alias filter. In the same figure, magnitude response of a 2-D FIR filter designed using impulse invariance response is shown. The kernel size of the 2-D FIR filter is  $51 \times 51$ . The ideal filter response has a passband area of 0.1207. The effective passband area, in which magnitude response is greater than 0.707 (half energy point), for the designed 2-D FIR filter is 0.1182.

We also designed a 2-D FIR filter assuming no crosstalk between the views. You would notice that this filter is more restrictive than the previous one. The shaded region in Fig. 4-4 (a) shows the passband of the ideal filter. Fig. 4-4 (a) also shows the contour plot of magnitude response of designed 2-D FIR filter using kernel size of  $51 \times 51$ . The ideal filter in this case has a passband area of 0.0912 as compared to effective passband area of 0.0940 for 2-D FIR filter.

In both the cases, the design of FIR filter is close to the ideal filter with very small transition band. The 3 dB contour line of FIR filter is reasonably close to the passband contour line of the ideal filter.

#### 4.4 Filter Design Results

In this section, we compare our anti-alias filters specifications with those obtained by filter specifications obtained by Konrad and Agniel (Konrad and Agniel, 2006). Fig. 4-5 (a) shows the passband of an ideal anti-alias filter using the non-orthogonal lattice model. The filter has a hexagonal passband that restricts the spatial frequencies almost equally in all the directions. Fig. 4-5 (b) shows the passband of an ideal anti-alias filter using the union of cosets model. The model approximates an individual view pixel pattern using union of 20 cosets. In this case, the ideal filter passband is more or less hexagonal but is more restrictive in some directions than other directions. In both cases, the sampling model used in filter design assumes that there is no crosstalk between the neighboring views.

Fig. 4-4 (a) shows the passband of the ideal filter, for a display with no crosstalk, designed using the method proposed in this chapter. The filter design is highly restrictive for diagonal frequencies, whereas it allows almost all the horizontal and vertical frequencies to pass through. The filter has a passband area of  $0.0912 = 1/10.96$  which is less than  $0.1111 (= 1/9)$ . This is because of irregular pixel distribution of the pixels

in individual views of the display. Though this kind of pixel distribution supports fewer frequencies without aliasing as compared to regular pixel distribution, loss of support happens in diagonal directions. Since the human eye is less sensitive to frequencies in diagonal directions, lack of diagonal frequencies on the display may not be perceived by an observer.

Fig. 4.4 (b) shows the passband of the ideal filter with crosstalk included in the model. The filter design is more or less similar to the filter design with no crosstalk case except the fact that this filter has a larger passband area. The passband area of ideal filter in this case is 0.1207 ( $= 1/8.29$ ) which is 32 percent more than the no-crosstalk case. The filter, as in the case of no crosstalk, is highly restrictive in diagonal directions but allows most of the horizontal and vertical frequencies in original images. In vertical direction, the bandwidth of the filter is 0.8 in normalized frequency. This means that even though we are downsampling our image by a factor of 9, the loss of frequency would be only 20 percent in vertical direction and 40 percent in horizontal direction.

Comparing our filter design with previous efforts (Konrad and Agniel, 2006), we see improvements in filter design due to the following reasons:

- The model to approximate an irregular pixel pattern is more mathematically accurate.
- The image spectrum is modeled using image covariance models.
- The crosstalk between neighboring views is taken into account.

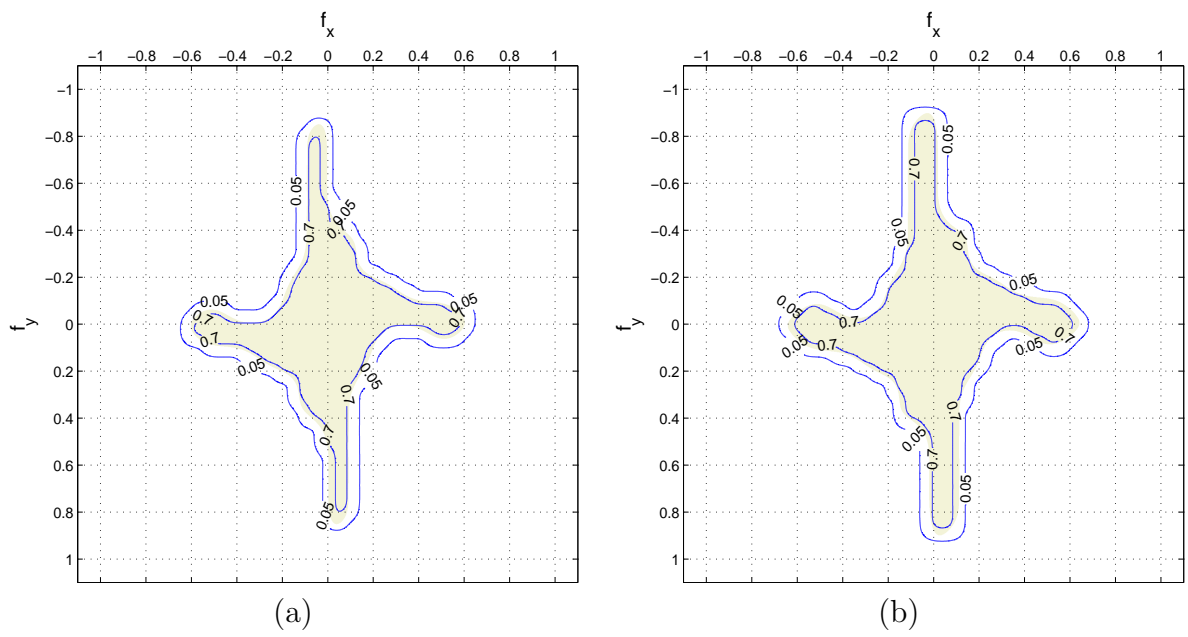


**Figure 4-4:** Contour plot of desired (shaded) and designed (contours) magnitude response for a multiplexing model based on irregular sampling in case of lenticular display: (a) with no crosstalk, and (b) with crosstalk. Note the wider passband in the case accounting for display crosstalk.

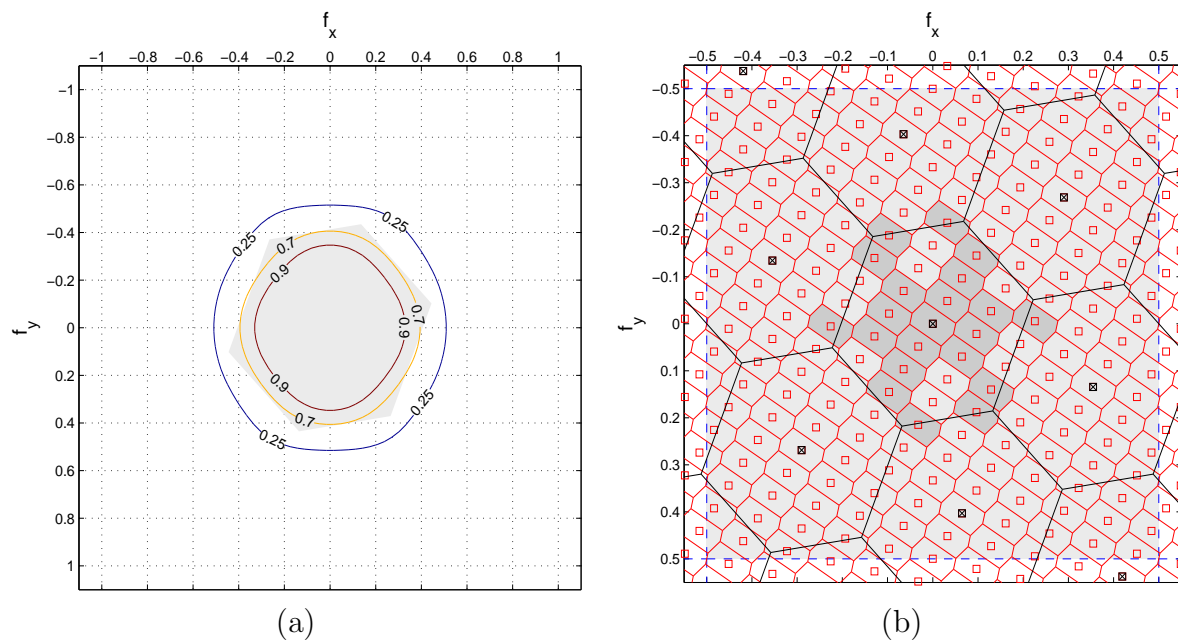


**Figure 4.5:** Contour plot of (a) desired (shaded) and designed (contours) magnitude response for a multiplexing model based on non-orthogonal lattice; and (b) desired response for model based on union of cosets (zoomed in be a factor of 2).

## Chapter 5

# Crosstalk Cancellation

In this chapter, we discuss our efforts to reduce “ghosting” or “blurring” effect in the lenticular autostereoscopic displays at object boundaries. We build a linear model of crosstalk for a lenticular automultiscopic display and use it to develop a crosstalk cancellation algorithm. The crosstalk model is quite similar to the one used by Klimenko (Klimenko et al., 2003a) and Konrad (Konrad et al., 2000). Our algorithm, unlike Klimenko’s (Klimenko et al., 2003a), tries to measure and cancel inter-ocular crosstalk rather than optical crosstalk. We later present the results obtained by our algorithm, by using 2 views and 3 views out of total 9 views, for Synthagram SG202.

### 5.1 Crosstalk Model

In this section, we build a crosstalk model for a spatially-multiplexed lenticular display. We begin with an assumption that our display has two views and later extend it to multiple views, that is, 9 views for the Synthagram SG202.

Since our display has only two views, for each eye one of them is intended and the other is an unintended view. Let us assume that view 1 is our intended view, and view 2 is our unintended view. Now we define the following terminology:

$I_1(x, y)$  is the true pixel pixel intensity at location  $(x, y)$  in view 1 of the display.

$I_2(\mathbf{x}_n, \mathbf{y}_n)$  is the intensity vector of a set of pixels of view 2 in the neighborhood of  $(x, y)$ .

$I'_1(x, y)$  is the observed pixel intensity at location  $(x, y)$  in view 1 of the display.

The optical crosstalk at  $(x, y)$  in view 1 occurs due to the pixels in neighborhood of  $(x, y)$  in view 2. So we can write the crosstalk model for the display as follows:

$$I'_1(x, y) = I_1(x, y) + \mathbf{a} * I_2(\mathbf{x}_n, \mathbf{y}_n) \quad (5.1)$$

Now if we assume that in view 2 pixels in neighborhood of  $(x, y)$  have the same intensities, as that of the pixel at location  $(x, y)$ , then

$$I_2(x, y) = I_2(\mathbf{x}_n, \mathbf{y}_n) \quad (5.2)$$

Using equation (5.1) and (5.2), we get:

$$I'_1(x, y) = I_1(x, y) + a_{12} * I_2(x, y) \quad (5.3)$$

The assumption in equation (5.2), makes our crosstalk model a simple one. Assuming that the crosstalk is symmetric, we write our crosstalk model equations for the two-view case as:

$$\begin{aligned} I'_1(x, y) &= I_1(x, y) + a_{12} * I_2(x, y) \\ I'_2(x, y) &= a_{12} * I_1(x, y) + I_2(x, y) \end{aligned} \quad (5.5)$$

The crosstalk equations can be written in matrix form as:

$$\begin{pmatrix} I'_1 \\ I'_2 \end{pmatrix} = \begin{pmatrix} 1 & a_{12} \\ a_{12} & 1 \end{pmatrix} \begin{pmatrix} I_1 \\ I_2 \end{pmatrix}$$

and

$$\mathbf{I}' = \mathbf{H} \times \mathbf{I}, \quad \mathbf{H} = \begin{pmatrix} 1 & a_{12} \\ a_{12} & 1 \end{pmatrix} \quad (5.7)$$

We extend the linear crosstalk model to 9 views as follows:

$$\mathbf{I}' = \mathbf{H} \times \mathbf{I}, \quad (5.8)$$

where  $\mathbf{H}$ ,  $\mathbf{I}$ , and  $\mathbf{I}'$  are defined below:

$$\mathbf{H} = \begin{bmatrix} a_{11} & a_{12} & \cdots & a_{19} \\ \vdots & \vdots & \ddots & \vdots \\ a_{91} & a_{92} & \cdots & a_{99} \end{bmatrix}$$

$$\mathbf{I} = [I_1 \ I_2 \ I_3 \ I_4 \ I_5 \ I_6 \ I_7 \ I_8 \ I_9]^T$$

$$\mathbf{I}' = [I'_1 \ I'_2 \ I'_3 \ I'_4 \ I'_5 \ I'_6 \ I'_7 \ I'_8 \ I'_9]^T$$

We use the linear crosstalk model in equation (5.8) to develop a crosstalk cancellation algorithm in the next section.

## 5.2 Crosstalk Cancellation Algorithm

We take an approach similar to the one taken in the development of crosstalk model (Section 5.1). We assume that our display has only two views and later extend it to multiple views. We develop a crosstalk algorithm which would cancel or reduce the "ghosting" effect due to the crosstalk.

We want to process original images  $\mathbf{I}$  in such a way that when these processed images are projected on the display, the images perceived by viewer would be the same as the original images. Since our crosstalk model is linear, a linear processing of original images would be sufficient to find an optimal solution.

Let  $\mathbf{G}$  be the processing matrix which is applied to the original images, then the processed images would be equal to:

$$\mathbf{I}_p = \mathbf{G}\mathbf{I} \quad (5.12)$$

The set of processed images is projected on the display, and they undergo crosstalk “addition” according to equation (5.8). The images viewed by an observer are:

$$\mathbf{I}_r = \mathbf{H}\mathbf{I}_p \quad (5.13)$$

Using equations (5.12), we get:

$$\mathbf{I}_r = \mathbf{H}\mathbf{G}\mathbf{I} \quad (5.14)$$

For a complete crosstalk cancellation, we would like to have  $\mathbf{I}_r = \mathbf{I}$ . If the matrix  $\mathbf{H}$  is a non-singular matrix, we get the following solution:

$$\mathbf{G} = \mathbf{H}^{-1} \quad (5.15)$$

Once we have computed the matrix  $\mathbf{G}$ , we can process our original images to obtain the processed images  $\mathbf{I}_p$  which can be displayed on the monitor after multiplexing them. The processed images however suffer from one problem; they have pixel values outside the range  $[0,255]$ . One solution to this problem is to saturate the values greater than 255 to 255 and negative values to 0. This makes our solution sub-optimal. A better approach is to perform a constrained linear least-squares minimization, i.e. to solve the following equation

$$\mathbf{I}_p = \underset{\mathbf{I}_p}{\operatorname{argmin}} \|\mathbf{I} - \mathbf{H}\mathbf{G}\mathbf{I}_p\|, \quad 0 \leq (\mathbf{I}_p)_i \leq 255, \text{ for all } i. \quad (5.16)$$

This gives us an optimal solution for the assumed crosstalk model. The problem with this solution is that it takes a lot of time to perform the optimization of each pair

of intensities. This, however, is not a problem because we can store the solution in a lookup table of size  $256 \times 256 \times 2$ , so the real processing time of the images is not affected.

The algorithm we developed performs uniform amount of crosstalk cancellation at every pixel. As discussed by Berkel (Berkel and Clarke, 1997), crosstalk actually improves image quality in datum plane, i.e., where the image has the same pixel values in all the views. This means that by performing crosstalk cancellation at pixels in datum plane, we are degrading the image quality. We know that crosstalk is a problem at object edges where "ghosting" or blurring of object edge boundaries occurs. So we would like to reduce crosstalk only at the edges.

The human visual system is sensitive to ratio of intensities and not the difference of intensities. This means a human observer would perceive the same difference between intensities 0.1 and 0.2, and 0.3 and 0.6. Hsu (Hsu et al., 1994) observed that crosstalk becomes perceivable only when the difference between image intensity is more than 14 percent. This means that perceived crosstalk between two views having intensities of 0.1 and 0.2 would be the same as between 0.3 and 0.6. We would like to make use of this characteristic of the human visual system in our crosstalk cancellation algorithm. This human visual characteristic has been quantitatively defined in Weber's law. Weber's law (Montag, 2002) states that "the ratio of the increment threshold to the background intensity is a constant." Though the physical crosstalk between views remains the same for range of image intensities from 0 to 255, the actual inter-ocular crosstalk varies depending on the image intensities of the views.

In a two-view display, let  $a_{12}$  be the crosstalk coefficient between the two views. We define  $r_{12}$  as a quantity which measures the difference between the image intensities with respect to the image with lower intensity,

$$r_{12} = \frac{|I_1 - I_2|}{\min(I_1, I_2) + \alpha} \quad (5.17)$$

The  $r_{12}$  measures the amount of “ghosting” between the images in a quantitative manner. The reason we want to measure with respect to lower intensity is that “ghosting” is more visible when you are looking at darker object than at brighter edge. For example, if two views have pixel values 100 and 200, then crosstalk is more visible in view 1 than in view 2. So the parameter  $r_{12}$  captures the amount of perceived crosstalk in the image with lower intensity. The data from Aguilar and Stiles (1954) (Montag, 2002) showed that for the Weber’s law to be true, a small baseline level of activity must be surpassed. The addition of  $\alpha$  in the denominator captures the fact that there is a low threshold activity which must be surpassed for this to be true. For example, suppose,  $I_1$  has value of 2 and  $I_2$  has value of 10. Although the ratio of intensity difference is 4 times larger than the lower intensity, the crosstalk is not actually visible. The value of  $\alpha$  measures the minimum level of activity which is needed for crosstalk to be visible. The value of  $\alpha$  was found experimentally.

Now, we use this parameter  $r_{12}$  to compute the amount of inter-ocular crosstalk. We assume that inter-ocular crosstalk varies linearly with the ratio of intensities and hence,

$$c_{12} = a_{12}r_{12} \quad (5.18)$$

The parameter  $c_{12}$  captures the amount of inter-ocular crosstalk; however when the value of  $r_{12}$  is greater than 1, then the value of  $c_{12}$  becomes greater than  $a_{12}$ . We limit our crosstalk cancellation algorithm to the maximum of amount of physical crosstalk present in the display. Hence, we get:

$$c_{12} = \min(a_{12} * r_{12}, a_{12}) \quad (5.19)$$

Now,  $c_{12}$  is used in our model, instead of  $a_{12}$ , to perform crosstalk cancellation. We build an  $\mathbf{H}$  matrix and use this matrix to do our crosstalk cancellation. We perform constrained linear least-squares minimization with upper bound as 255 and lower bound as 0 as in equation (5.16).

This algorithm can be easily extended to multiple views. We use the algorithm to perform crosstalk cancellation on the automultiscopic display Synthagram SG202.

$$r_{ij} = \frac{|I_i - I_j|}{\min(I_i, I_j) + \alpha} \quad (5.20)$$

$$c_{ij} = \min(a_{ij} * r_{ij}, a_{ij}) \quad (5.21)$$

The modified crosstalk cancellation coefficient can be plugged into our crosstalk model using equation (5.8) to process the images. Tables 4.1 and 4.2 give the measured physical crosstalk coefficients  $a_{ij}$ .

<i>View No. →</i>	1	2	3	4	5	6	7	8	9
<i>Crosstalk ratio: 1Q</i>	1.000	0.745	0.085	0.008	0.003	0.003	0.004	0.025	0.305
<i>Crosstalk ratio: 2Q</i>	1.000	0.208	0.014	0.003	0.002	0.003	0.014	0.202	0.984
<i>Crosstalk ratio: 3Q</i>	1.000	1.261	0.412	0.024	0.004	0.003	0.004	0.018	0.215
<i>Crosstalk ratio: 4Q</i>	1.000	0.338	0.031	0.005	0.003	0.004	0.017	0.229	0.894

**Table 5.1:** Spatially-variant crosstalk measurements with view 1 as center

<i>View No. →</i>	1	2	3	4	5	6	7	8	9
<i>Crosstalk ratio: 1Q</i>	0.017	0.269	1.000	0.741	0.086	0.076	0.002	0.001	0.03
<i>Crosstalk ratio: 2Q</i>	0.157	1.039	1.000	0.172	0.011	0.003	0.002	0.003	0.012
<i>Crosstalk ratio: 3Q</i>	0.012	0.159	1.000	1.396	0.491	0.029	0.004	0.002	0.003
<i>Crosstalk ratio: 4Q</i>	0.171	0.898	1.000	0.353	0.035	0.004	0.002	0.003	0.013

**Table 5.2:** Spatially-variant crosstalk measurements with view 3 as center.

### 5.3 Applying Crosstalk Cancellation Algorithm

The Synthagram SG202 has total of nine views. However, we would like to test our algorithm by first illuminating 2 views, then 3 views and then illuminating all 9 views. In this experiment, we use only 2 views while the remaining 7 views contain zero intensities. The actual values used in the model were (Tables 4.1 and 4.2):

$$a_{12} = 0.6, \alpha = 10 \quad (5.22)$$

In order to speed up the algorithm, we created a look up table of size  $256 \times 256 \times 2$  which stores the results of crosstalk cancellation algorithm for all possible pairs of image intensities. We use the lookup table to process the images and then multiplex the processed images in a normal way.

Unfortunately, our display is not spatially uniform; the degree of crosstalk is different in the four corners of the screen. Therefore, our next step is to model spatial variation of crosstalk coefficient across the display. We divided the display into four separate zones: Top-left, Top-right, Bottom-left, and Bottom-right. In each of the zones, the crosstalk coefficient was assumed to be spatially invariant. We used a different coefficient for different zone. The four zonal coefficients shown in Tables 5.1 and 5.2. They were estimated in the same manner as those in Tables 4.1 and 4.2.

We, now, test the algorithm by illuminating only 3 while the remaining 6 views contain zero intensities. The actual values used in the crosstalk cancellation algorithm were:

$$a_{12} = 0.6, a_{23} = 0.6, a_{13} = 0.12, \alpha = 10 \quad (5.23)$$

To improve the speed, we create a lookup table of size  $(256, 256, 256, 3)$  which stores the results of crosstalk-cancelled triplets. Performing the optimization over 16581120

( $=256*256*257/2$ ) triplets of intensities becomes time consuming. To reduce the processing time, optimization results were computed for several points uniformly-distributed all over the domain in step of 5, and then nearest-neighbor interpolation was performed for other intensity triplets.

This lookup table was used for processing the original images and multiplexed in the normal way. Similar to the two-view case, we used our model of spatial variation of optical crosstalk coefficients over the display. This would give better results than using spatially-uniform coefficients.

Finally, we used all 9 views of our display. The coefficient values in the model are the same as given in Tables 4.1 and 4.2. The nine-view model requires performing a large number of optimization, i.e., over  $\binom{256}{9}$  intensities tuples. This is a very large number and even if we decide to perform optimization over selected points, it would still be unmanageable unless the selected points are far apart. We need to develop an efficient and reasonably accurate solution to this problem.

## 5.4 Results

In this section, we present the results of crosstalk cancellation algorithm applied to Synthagram SG202 using 2 views and 3 views.

- The object boundaries became a little bit sharper with reduced level of ghost images.
- The images overall looked sharper than the images without any processing.
- The overall brightness of images remains more or less unchanged, as the crosstalk cancellation algorithm performed a selective cancellation at the object edges.
- The quality of objects in the datum plane, where crosstalk actually results in higher image resolution, remained the same.

- The crosstalk cancellation algorithm improved the quality of images.

## Chapter 6

# Conclusion

### 6.1 Discussion of Results

In Chapters 2, 3, and 4, we proposed a filter design method which can handle irregular sampling structure and crosstalk between the views. The model resulted in design of anti-alias filter whose frequency response primarily attenuates diagonal frequencies and leaves horizontal and vertical frequencies intact. The filter design works marginally better than the non-orthogonal lattice model (Konrad and Agniel, 2006). The improvement obtained was not much because of the fact that most of the natural images do not have very high frequency content. In such a case, any filter with cutoff frequencies within an appropriate range would be able to do a reasonable job of removing aliasing artifacts. However, there are some visible improvements in areas which contain diagonal frequencies. The human eye is not very sensitive to diagonal frequencies; this minor improvement comes at the cost of increased number of coefficients in 2-D FIR filter and makes separable filter design very difficult. Also, in the case of moving pictures the aliasing artifacts are less perceptible so separable orthogonal filter may do a reasonable job.

Though the proposed method to design gave minimal improvements, it can be used to design anti-aliasing filter for any system which performs downsampling from regular to irregular sampling structure. In the case when the signal spectrum is not known, it is possible to design anti-alias filter, except that it would not result in optimal design.

In the crosstalk cancellation algorithm, we developed a linear model for crosstalk and used it to perform crosstalk cancellation. The algorithm uses a lookup table to perform crosstalk cancellation for the two-view and three-view case and hence can be used to perform real-time crosstalk cancellation. The crosstalk cancellation algorithm improved the sharpness of the image for the 2 and 3-view cases.

## 6.2 Suggestions for Further Work

In case of anti-alias filter design for the SG202 display, we can explore the possibility of analyzing the image spectrum and designing the filter in real time. This might result in better image quality and reduce the aliasing artifacts further. The current systems may not be able to support real-time filter design but as the processing power of desktops increases it might be possible in the future.

The current filter design methodology assumes crosstalk to be spatially invariant. However this is not true, so it would be a good idea to include spatial variation of crosstalk coefficients in the sampling model to improve accuracy of filter design.

We implemented crosstalk cancellation algorithm for 2 and 3-view cases and the next logical step is to implement it for the 9-view case. Since, it is not possible to perform optimization for a large number of tuples, it is necessary to find a solution which gives us reasonable solution for the crosstalk model.

In our crosstalk cancellation model, the crosstalk coefficients were considered to be spatially invariant. The best we did was dividing the monitor into four zones, and then assumed invariance of crosstalk coefficients within the zones. One possibility is to approximate the spatial variation of crosstalk coefficients with some polynomial or spline function and use it in our crosstalk reduction algorithm.

We assumed in our crosstalk model, that the image crosstalk happens between the views pixels at the same location in space. This, however, can be better modeled if

we incorporate the fact that crosstalk happens from neighboring pixels. The next step to improve the crosstalk cancellation algorithm would be to perform joint crosstalk cancellation between a set of neighboring pixels.



## References

- Agniel, P. (2004). Subsampling models and anti-alias filters for 3-d automulti-  
scopic displays. *M.S. Thesis, Boston University*.
- Aurenhammer, F. (1991). Voronoi diagrams - a survey of a fundamental geo-  
metric data structure. *ACM Computing Surveys.*, 23:345–405.
- Berkel, C. V. (1999). Image preparation for 3d lcd. *In proceedings of SPIE  
Stereographics Displays and Virtual Reality Systems.*, 3639:84–91.
- Berkel, C. V. and Clarke, J. A. (1997). Characterisation and optimisation of  
3d-lcd module design. *In proceedings of SPIE*, 3012:179–186.
- Berkel, C. V., Franklin, A., and Mansell, J. (1996a). Design and application of  
of multiview 3d lcd. *In proceedings of SID Euro-Display.*, pages 109–112.
- Berkel, C. V., Parker, D. W., and Franklin, A. (1996b). Multiview 3d-lcd.  
*In proceedings of SPIE Stereographics Displays and Virtual Reality Systems.*,  
2653:32–39.
- Cossairt, O. S. (2003). A view-sequential 3d display. *M.S. Thesis, MIT*.
- Dodgson, N. A. (2005). Autostereoscopic 3d displays. *Computer: IEEE*, 38:31–  
36.
- Dubois, E. (1985). The sampling and reconstruction of time-varying imagery  
with application in video systems. *In Proceedings of the IEEE*, 73(4):502–522.
- Dubois, E. (2001). A projection method to generate anaglyph stereo images.  
*Proceedings of IEEE Int. Conf. Acoustics Speech Signal Processing.*, 3:1661–  
1664.
- Holliman, N. (2005). 3d displays systems. *Technical Report, Department of  
Computer Science, University of Durham*.
- Hsu, J., Pizlo, Z., Babbs, C. F., Chelberg, D., and Delp, E. (1994). Design  
of studies to test the effectiveness of stereo imaging truth or dare: is stereo  
viewing really better? *In proceedings of SPIE*, 2177:211–222.

- Klimenko, S., Frolov, P., Nikitina, L., and Nikitin, I. (2003a). Crosstalk reduction in passive stereo-projection systems. *In proceedings of Eurographics 2003*, pages 235–240.
- Klimenko, S. V., Nikitin, I., and Nikitina, L. (2003b). Reducing optical crosstalk in affordable systems of virtual environment. *Second International Conference on Cyberworlds*, page 100.
- Konrad, J. and Agniel, P. (2003). Artifact reduction in lenticular multiscopic 3-d displays by means of anti-alias filtering. *In proceedings of SPIE Stereoscopic Displays and Virtual Reality Systems*, 5006A:336–347.
- Konrad, J. and Agniel, P. (2004). Non-orthogonal sub-sampling and anti-alias filtering for multiscopic 3-d displays. *In proceedings of SPIE Stereoscopic Displays and Virtual Reality Systems*, 5291:105–116.
- Konrad, J. and Agniel, P. (2006). Subsampling models and anti-alias filters for 3-d automultiscopic displays. *IEEE transaction of Image processing*, 15:128–140.
- Konrad, J., Lacotte, B., and Dubois, E. (2000). Cancellation of image crosstalk in time-sequential displays of stereoscopic video. *IEEE transactions on Image processing*, 9:897–908.
- Lipscomb, J. and Wooten, W. (1994). Reducing crosstalk between stereoscopic views. *Proceedings of SPIE.*, 2177:92–96.
- Mayhew, J. E. W. and Longuet-Higgins, H. C. (1982). A computational model of binocular depth perception. *Nature.*, 297:376–378.
- Montag, E. D. (2002). Weber’s law. [http://www.cis.rit.edu/people/faculty/montag/vandplite/pages/chap\\_3/ch3%p1.html](http://www.cis.rit.edu/people/faculty/montag/vandplite/pages/chap_3/ch3%p1.html).
- Pommeray, M., Kastelik, J.-C., and Gazalet, M. G. (2003). Image crosstalk reduction in stereoscopic laser-based display systems. *Journal of Electronic Imaging*, 12:689–696.
- Rogers, B. and Graham, M. (1982). Similarities between motion parallax and stereopsis in human depth perception. *Vision Research*, 22(2):261–270.
- Stereographics (2003). Stereographics developer’s handbook. *Stereographics Corporation*.
- Woods, A. and Tan, S. (2002). Characterising sources of ghosting in time-sequential stereoscopic video displays. *Stereoscopic Displays and Virtual Reality Systems IX, Proceedings of SPIE*, 4660:66–77.

- Yeh, Y. and Silverstein, L. (1990). Limits of fusion and depth judgement in stereoscopic colour displays. *Human Factors*, 32(1):45–60.
- Zayed, A. (1996). *Handbook of Function and Generalized Function Transformations*. CRC-Press.
- Zemanian, A. (1987). *Distribution Theory and Transform Analysis : An Introduction to Generalized Functions, with Applications*. Dover Publications.



**ASHISH JAIN**  
80 Gordon Street, Apt 7  
Brighton, MA 02135  
send2ashish@yahoo.com  
Phone: 617-304-3432

## **EDUCATION**

- Master in Science, Electrical Engineering: Signal processing and Communication (Sept 2004 - till date) Boston University 3.96/4.0
- Bachelor of Technology, Electronics and Electrical Communication Engineering. IIT Kharagpur 8.44/10

## **ACADEMIC AWARDS AND ACHIEVEMENTS**

- Awarded Graduate Teaching Fellowship for MS program in Electrical engineering at Boston University.
- Secured All India Rank 466 in IIT Joint Entrance Examination among 110,000 applicants.
- Secured All India 13th rank in Madhya Pradesh Pre Engineering test among 48000 applicants.
- Awarded National Talent Search Scholarship, among 750 students all over India.
- Awarded scholarship for being among top 0.1 percent students in science by CBSE, New Delhi.

## **SKILLS**

- Programming Languages: C, MATLAB, Verilog.
- Operating systems: Unix, Win 9x/XP/2000.
- Assembly languages: TMS C55x, TMS C54x, ARM9.